RESEARCH ARTICLE | JUNE 06 2025

# A projection method to symmetrize the momentum flux in a vector lattice Boltzmann formulation of hydrodynamics

**Special Collection:** Proceedings of the 33rd Conference on Discrete Simulation of Fluid Dynamics

Paul J. Dellar



*Physics of Fluids* 37, 063606 (2025)
https://doi.org/10.1063/5.0268328

Physics of Fluids ARTICLE pubs.aip.org/aip/pof

# A projection method to symmetrize the momentum flux in a vector lattice Boltzmann formulation of hydrodynamics

Cite as: Phys. Fluids **37**, 063606 (2025); doi: 10.1063/5.0268328
Submitted: 28 February 2025 · Accepted: 19 April 2025 ·
Published Online: 6 June 2025



Paul J. Dellar[a)]

## AFFILIATIONS

Mathematical Institute, University of Oxford, Radcliffe Observatory Quarter, Oxford OX2 6GG, United Kingdom

**Note:** This paper is part of the Special Topic, Proceedings of the 33rd Conference on Discrete Simulation of Fluid Dynamics.
[a)]**Author to whom correspondence should be addressed:** paul.dellar@maths.ox.ac.uk

## ABSTRACT

The standard lattice Boltzmann approach to hydrodynamics uses scalar distribution functions to represent the number densities of particles. Each particle moves with one of a small set of constant velocities. The momentum flux is the second moment of these distribution functions with respect to the particle velocities. The momentum flux is thus a symmetric tensor by construction, so the conservation law for linear momentum implies a conservation law for angular momentum. A more flexible approach uses vector distribution functions instead. Each particle carries a momentum that may not be aligned with its direction of propagation. The momentum flux tensor is in general not symmetric, so the evolution equation for angular momentum contains a source term as well as a flux. The momentum flux can be symmetrized using a more general model for collisions between particles that applies separate relaxation times to the symmetric and antisymmetric parts of the momentum flux and then sets the relaxation time for the antisymmetric part to zero. The resulting algorithm is equivalent to a projection of the momentum flux onto the space of symmetric tensors, analogous to the Chorin–Temam projection scheme for the incompressible Navier–Stokes equations that projects the velocity field onto the space of divergence-free vector fields.





## I. INTRODUCTION

A conservation law for linear momentum underpins most of continuum mechanics, in particular the Navier–Stokes equations that describe Newtonian fluids. The momentum flux is almost always taken to be a symmetric rank-2 tensor. A conservation law for angular momentum then follows directly from the conservation law for linear momentum. However, the conservation laws for linear and angular momentum in deformable continuous media are, in principle, independent. Truesdell attributed this realization to Euler in 1775.[1–4] Hamel[5] named the symmetry of the momentum flux the "Boltzmann axiom" following Boltzmann's writings on continuum mechanics,[6] while Truesdell and Toupin[7] named it "Cauchy's second law." The former name better reflects a property that holds for many, but not all, continuous media. There is a common argument, dating back to Stokes, that arbitrarily small material volumes will experience arbitrarily large angular accelerations unless the momentum flux is symmetric.[8,9] This argument is incorrect because it assumes the general validity of an angular momentum conservation law that only holds when the momentum flux is symmetric. Thomson[10] devised a mechanical model with a collection of gyroscopes to show that the macroscopic stress tensor for a medium with microstructure may be antisymmetric.

The lattice Boltzmann method represents a fluid using particles.[11–14] Each particle moves with one of a finite set of velocities, chosen so that all particles move synchronously from one lattice point to another lattice point over a finite time step. Particles collide in a stylized way at lattice points while conserving momentum and particle number. The numbers of particles are represented by a finite set of scalar distribution functions, one for each velocity, that are themselves functions of position and time. These functions evolve according to a linear, constant-coefficient hyperbolic system with nonlinear algebraic source terms. The momentum density and momentum flux are equal to the first and second moments of the distribution functions with respect to the particle velocities. The momentum flux is then symmetric by construction and so automatically satisfies the Boltzmann axiom.

The representation of a vector field as the first moment of scalar distribution functions, and its flux by the second moment, is too limited to describe electromagnetic fields governed by Maxwell's

equations. Instead, these fields have been described using sets of tensor or vector distribution functions.[15–20] The tensor approach describes the fluid and the electromagnetic field using different moments of a single set of tensor distribution functions.[15] The vector approach is more modular, using vector distribution functions to describe the electromagnetic field alone and a conventional lattice Boltzmann formulation using a second set of scalar distributions to describe the fluid.[17–20] The vector approach was inspired by Bouchut's kinetic formulation of a general hyperbolic system of conservation laws using continuous distribution functions with one component for each conserved variable in the hyperbolic system.[21] It can also describe the evolving orientations of axisymmetric particles in suspensions.[22]

Carfora and Natalini[23] constructed a discrete kinetic formulation for hydrodynamics using the vector approach. This has recently been used as the basis for multidimensional lattice Boltzmann schemes by Zhao,[24] Baty *et al.*,[25] and Wissocq *et al.*,[26] following earlier one-dimensional schemes by Dubois and Graille.[27,28] The natural vector formulation is unstable and can only be stabilized by rescaling the relation between fluxes and conserved quantities. For example, the mass flux is normally equal to the momentum density, but in this formulation the two are related by a multiplicative constant chosen to ensure stability. The constant can be absorbed by rescaling the time coordinate. The incompressible Navier–Stokes equations are then recovered exactly in the incompressible limit. However, only the divergence of the momentum flux is correct. The momentum flux itself differs from the momentum flux in a Newtonian fluid and is not even a symmetric tensor. This vector kinetic formulation of hydrodynamics therefore does not satisfy the Boltzmann axiom. The usual conservation law for angular momentum does not hold, even in the incompressible limit.

The same issue arises in another hydrodynamic simulation technique inspired by kinetic theory, called multiparticle collision dynamics,[29–31] or stochastic rotation dynamics.[32,33] Part of the simulated momentum flux has the same asymmetry as in vector lattice Boltzmann hydrodynamics.[34,35] This asymmetry causes artifacts in simulations of flows driven by boundary torques and in flows of mixtures of fluids with different viscosities.[36]

The purpose of this paper is to describe a collision operator with a separately adjustable "vortex viscosity" for the antisymmetric part of the momentum flux in vector lattice Boltzmann hydrodynamics. One can set the vortex viscosity to zero and recover the usual angular momentum conservation law for a continuous medium with a symmetric momentum flux tensor. Diffusion coefficients have been set to zero before to remove dissipation in lattice Boltzmann formulations for the scalar wave equation and Maxwell's equations,[16,18] and for palindromic relaxation schemes for hyperbolic systems.[37] The surprise is that a kinetic formulation for nonlinear hydrodynamic equations remains stable with zero vortex viscosity, that one can construct consistent initial conditions, and that one can diagnose the fluid vorticity locally at lattice points. The resulting algorithm can be interpreted as a projection scheme, analogous to the Chorin–Temam projection scheme for simulating the incompressible Navier–Stokes equations.[38,39]

## II. LINEAR AND ANGULAR MOMENTUM CONSERVATION IN CONTINUUM MECHANICS

Conservation of linear momentum in a deformable continuous medium can be expressed very generally by requiring that Newton's second law for a material volume $\mathcal{V}$ takes the form

$$\frac{\mathrm{d}}{\mathrm{d}t}\int_V \rho\mathbf{u}\,\mathrm{d}V = \int_{\partial V} \mathbf{n}\cdot\boldsymbol{\sigma}\,\mathrm{d}S, \tag{1}$$

where $\boldsymbol{\sigma}$ is the Cauchy stress tensor, and $\mathbf{n}$ is the outward-pointing unit normal on the boundary $\partial V$. The momentum density $\rho\mathbf{u}$ is conventionally written as the product of the mass density $\rho$ and the fluid velocity $\mathbf{u}$. The tensor contraction is between the left index of $\boldsymbol{\sigma}$ and the outward normal vector $\mathbf{n}$ on the surface $\partial V$, so $\mathbf{n}\cdot\boldsymbol{\sigma}$ is the traction force per unit area exerted on a piece of the boundary $\partial V$ by the fluid toward which $\mathbf{n}$ points.

Introducing the momentum flux tensor $\boldsymbol{\Pi} = \rho\mathbf{u}\mathbf{u} - \boldsymbol{\sigma}$ and using Reynolds' transport theorem leads to the analogous statement

$$\frac{\mathrm{d}}{\mathrm{d}t}\int_V \rho\mathbf{u}\,\mathrm{d}V = -\int_{\partial V} \mathbf{n}\cdot\boldsymbol{\Pi}\,\mathrm{d}S \tag{2}$$

for any fixed volume $V$ of space. This is equivalent to the local momentum conservation law

$$\partial_t(\rho\mathbf{u}) + \nabla\cdot\boldsymbol{\Pi} = 0 \tag{3}$$

via the divergence theorem. For example, taking $\boldsymbol{\Pi} = pI + \rho\mathbf{u}\mathbf{u}$, where I is the identity tensor, gives the Euler equation for a compressible ideal fluid with pressure $p$. Writing $\mathbf{n}$ on the left of $\boldsymbol{\sigma}$ and $\boldsymbol{\Pi}$ in (1) and (2) is necessary if one wants to write the local momentum conservation law in the divergence form (3) without assuming $\boldsymbol{\sigma}$ to be symmetric. This convention is commonly (though not universally) used when $\boldsymbol{\sigma}$ need not be symmetric.[4,40,41]

Forming the vector product between the position vector $\mathbf{x}$ and the momentum conservation equation (3) gives

$$\partial_t(\mathbf{x}\times\rho\mathbf{u}) + \mathbf{x}\times\nabla\cdot\boldsymbol{\Pi} = 0. \tag{4}$$

This is an evolution equation for angular momentum about the origin, but we can freely replace $\mathbf{x}$ with $\mathbf{x}-\mathbf{x}_0$ for any constant vector $\mathbf{x}_0$ to formulate an evolution equation for angular momentum about an arbitrary point $\mathbf{x}_0$. Equation (4) can be written in index notation as

$$\partial_t(\epsilon_{\alpha\beta\gamma}x_\beta\rho u_\gamma) + \epsilon_{\alpha\beta\gamma}x_\beta\partial_\delta\Pi_{\delta\gamma} = 0. \tag{5}$$

We use Greek indices for vector and tensor components, reserving Roman indices for discrete velocities later. The derivative $\partial_\delta = \partial/\partial x_\delta$ contracts with the left index of $\boldsymbol{\Pi}$. Adding $\epsilon_{\alpha\beta\gamma}(\partial_\delta x_\beta)\Pi_{\delta\gamma}$ to both sides gives

$$\partial_t(\epsilon_{\alpha\beta\gamma}x_\beta\rho u_\gamma) + \partial_\delta(\epsilon_{\alpha\beta\gamma}x_\beta\Pi_{\delta\gamma}) = \epsilon_{\alpha\beta\gamma}\Pi_{\beta\gamma}. \tag{6}$$

The left-hand side now contains the divergence of an angular momentum flux, but there is a source term on the right-hand side involving the antisymmetric part of $\boldsymbol{\Pi}$. We can rewrite (6) in vector notation as

$$\partial_t(\mathbf{x}\times\rho\mathbf{u}) + \nabla\cdot(-\boldsymbol{\Pi}\times\mathbf{x}) = \boldsymbol{\epsilon}:\boldsymbol{\Pi}. \tag{7}$$

The vector on the right-hand side is a double tensor contraction between the alternating tensor $\boldsymbol{\epsilon}$ and the momentum flux $\boldsymbol{\Pi}$. Integrating (7) over a space-fixed volume $V$ gives

$$\frac{\mathrm{d}}{\mathrm{d}t}\int_V \mathbf{x}\times\rho\mathbf{u}\,\mathrm{d}V = \int_{\partial V}\mathbf{n}\cdot\boldsymbol{\Pi}\times\mathbf{x}\,\mathrm{d}S + \int_V \boldsymbol{\epsilon}:\boldsymbol{\Pi}\,\mathrm{d}V, \tag{8}$$

where $\mathbf{n}$ is the outward-pointing unit normal on the boundary $\partial V$. When $\boldsymbol{\Pi}$ is symmetric, this takes the more familiar form

$$\frac{\mathrm{d}}{\mathrm{d}t}\int_V \mathbf{x}\times\rho\mathbf{u}\,\mathrm{d}V = -\int_{\partial V}\mathbf{x}\times\mathbf{\Pi}\cdot\mathbf{n}\,\mathrm{d}S, \tag{9}$$

but in general there is also a volume integral of $\boldsymbol{\epsilon}:\mathbf{\Pi}$ on the right-hand side. No large angular accelerations arise from applying (8) to small material volumes when $\mathbf{\Pi}$ is not symmetric. The leading-order contributions from the surface and volume integrals on the right-hand side cancel.

To construct a new angular momentum conservation law with the same structural form as (4), we postulate the existence of an internal angular momentum density described by a vector field $\mathbf{s}$ that evolves according to[42–44]

$$\partial_t(\rho\mathbf{s}) + \nabla\cdot\mathbf{C} = -\boldsymbol{\epsilon}:\mathbf{\Pi}. \tag{10}$$

The tensor $\mathbf{C}$ is called the couple flux (or couple stress) by analogy with the momentum flux $\mathbf{\Pi}$. The need to introduce an internal angular momentum density $\mathbf{s}$ is analogous to the need to introduce an internal energy density proportional to the local temperature when deriving a hydrodynamic energy conservation equation from the Boltzmann equation.

Adding (7) and (10) gives a local conservation law for the total angular momentum density

$$\partial_t(\mathbf{x}\times\rho\mathbf{u} + \rho\mathbf{s}) + \nabla\cdot(-\mathbf{\Pi}\times\mathbf{x} + \mathbf{C}) = 0. \tag{11}$$

The internal angular momentum density $\rho\mathbf{s}$ is often called the "spin," while $\mathbf{x}\times\rho\mathbf{u}$ is called the "orbital" angular momentum density. These names come from the properties of angular momentum in quantum mechanics. In suspensions, the spin is due to rotation of the suspended particles relative to the fluid around them.[41,45] The antisymmetric part of $\mathbf{\Pi}$ is responsible for exchanging angular momentum between $\rho\mathbf{s}$ and $\mathbf{x}\times\rho\mathbf{u}$. The spin and orbital angular momenta are each separately conserved when $\mathbf{\Pi}$ is symmetric.

The momentum flux tensor $\mathbf{\Pi} = \int\boldsymbol{\xi}\boldsymbol{\xi}f(\mathbf{x},\boldsymbol{\xi},t)\,\mathrm{d}\boldsymbol{\xi}$ is symmetric by construction in Boltzmann's description of a rarefied monatomic gas. The distribution function $f(\mathbf{x},\boldsymbol{\xi},t)$ represents the number density of particles at position $\mathbf{x}$ and time $t$ moving with velocity $\boldsymbol{\xi}$. The assumption that the momentum flux $\mathbf{\Pi}$ should be symmetric in continuum mechanics, as formulated from first principles without any underlying kinetic description, was named the "Boltzmann axiom" by Hamel[5] following Boltzmann's writings on continuum mechanics.[6] The subsequent development of a kinetic theory for diatomic gases greatly influenced the development of continuum theories for media with internal angular momentum.[42,46,47]

## III. HYDRODYNAMICS WITH VORTEX VISCOSITY

Having allowed $\mathbf{\Pi}$ to be asymmetric, it is natural to extend the constitutive relation for a Newtonian fluid to[42,45,48–50]

$$\begin{aligned}\Pi_{\alpha\beta} = {}& p\delta_{\alpha\beta} + \rho u_\alpha u_\beta - \mu_\nu\left(\frac{\partial u_\beta}{\partial x_\alpha} - \frac{\partial u_\alpha}{\partial x_\beta} - 2\epsilon_{\alpha\beta\gamma}\Omega_\gamma\right)\\ & - \mu_s\left(\frac{\partial u_\alpha}{\partial x_\beta} + \frac{\partial u_\beta}{\partial x_\alpha} - \frac{2}{D}\frac{\partial u_\gamma}{\partial x_\gamma}\delta_{\alpha\beta}\right) - \mu_b\left(\frac{\partial u_\gamma}{\partial x_\gamma}\right)\delta_{\alpha\beta},\end{aligned} \tag{12}$$

in $D$ spatial dimensions. The coefficients include a vortex viscosity $\mu_\nu$ as well as the usual shear viscosity $\mu_s$ and bulk viscosity $\mu_b$. This grouping into a sum of antisymmetric, symmetric and traceless, and isotropic terms is the most general decomposition of a rank-2 tensor that is irreducible under rotations. Molecular dynamics simulations of water at various temperatures using a flexible single point charge[51] model yield a vortex viscosity that is between 19% and 33% of the shear viscosity.[52]

However, the vortex viscous term contains a contribution from an internal angular velocity field $\mathbf{\Omega}$. This is needed to make the constitutive relation (12) invariant under time-dependent rigid-body rotations. The internal angular velocity is typically related to the internal angular momentum by $\mathbf{s} = \mathscr{I}\mathbf{\Omega}$ for an isotropic medium, where $\mathscr{I}$ is the average moment of inertia per unit mass associated with the internal angular degrees of freedom. The factor of 2 in the $\Omega_\gamma$ terms arises because the vorticity is twice the local angular velocity, i.e., $\nabla\times(\mathbf{\Omega}\times\mathbf{x}) = 2\mathbf{\Omega}$ when $\mathbf{\Omega}$ is a constant vector.

The linear momentum conservation law corresponding to (12) can be written as[48,49]

$$\begin{aligned}\partial_t(\rho\mathbf{u}) + \nabla\cdot(\rho\mathbf{u}\mathbf{u}) + \nabla p = {}& (\mu_s+\mu_\nu)\nabla^2\mathbf{u}\\ & + (\mu_s/D + \mu_b - \mu_\nu)\nabla(\nabla\cdot\mathbf{u})\\ & + 2\mu_\nu\nabla\times\mathbf{\Omega}\end{aligned} \tag{13}$$

if the viscosity coefficients are all constants. The corresponding evolution equation (10) for $\mathbf{s}$ becomes[41,49]

$$\rho\mathscr{I}(\partial_t + \mathbf{u}\cdot\nabla)\mathbf{\Omega} = 2\mu_\nu(\nabla\times\mathbf{u} - 2\mathbf{\Omega}) + \nu_1\nabla^2\mathbf{\Omega} + \nu_2\nabla(\nabla\cdot\mathbf{\Omega}). \tag{14}$$

The "spin viscosity" coefficients $\nu_1$ and $\nu_2$ relate the couple flux $\mathbf{C}$ to $\nabla\mathbf{\Omega}$ and its transpose. The internal angular velocity then typically relaxes toward half the fluid vorticity on a timescale $\mathscr{T} = \mu_\nu/(\rho\mathscr{I})$. This timescale is typically very short, in the sense that $\mathscr{T}|\nabla\times\mathbf{u}| \ll 1$, so the effect of the vortex viscous term is very small even when the vortex viscosity $\mu_\nu$ is not itself small compared with the shear viscosity $\mu_s$. Exceptions can arise in boundary layers as the $\nu_1$ and $\nu_2$ terms become significant on sufficiently small lengthscales.[52]

Moreover, the vortex viscous term vanishes for a steady rigid-body rotation with velocity field $\mathbf{u} = \mathbf{W}\times\mathbf{x}$. The internal angular velocity $\mathbf{\Omega}$ will be spatially uniform and equal to $\mathbf{W}$. The conventional symmetric viscous terms also vanish for this flow, so there is no viscous dissipation. Including the $\Omega_\gamma$ term in (12) circumvents Landau and Lifshitz's argument that the vortex viscosity must vanish to ensure zero viscous dissipation under rigid-body rotations.[53]

## IV. VECTOR LATTICE BOLTZMANN FORMULATIONS OF HYDRODYNAMICS

The vector lattice Boltzmann algorithms studied by Zhao[24] and Baty *et al.*[25] use the representations

$$\rho = \sum_{i=0}^{N-1} f_i, \quad \rho\mathbf{u} = \sum_{i=0}^{N-1}\mathbf{g}_i, \tag{15}$$

with a set of scalar distribution functions $f_0,\ldots f_{N-1}$ for the mass density, and a second set of vector distribution functions $\mathbf{g}_0,\ldots,\mathbf{g}_{N-1}$ for the momentum density. These can be combined into a single set of vector distribution functions $\mathbf{F}_i = (f_i,\mathbf{g}_i)$, each with $D+1$ components in $D$ spatial dimensions, following Bouchut's formulation for general hyperbolic systems.[21] However, the derivation of the hydrodynamic equations is simpler if we keep the $f_i$ and $\mathbf{g}_i$ distribution functions separate.

The stability of the vector lattice Boltzmann formulation for hydrodynamics relies on a rescaling of the discrete particle velocities

relative to the standard scalar formulation. Taking $\boldsymbol{\xi}_i$ to be the usual discrete velocities of the D2Q5 lattice

$$\boldsymbol{\xi}_0 = (0,0), \quad \boldsymbol{\xi}_1 = (1,0), \quad \boldsymbol{\xi}_2 = (0,1), \quad \boldsymbol{\xi}_3 = (-1,0), \quad \boldsymbol{\xi}_4 = (0,-1), \tag{16}$$

we define a rescaled set of discrete velocities

$$\mathbf{c}_i = \lambda \boldsymbol{\xi}_i. \tag{17}$$

The constant $\lambda$ must be larger than 2 for stability (see the Appendix). The scalar and vector distribution functions are now postulated to evolve according to the kinetic equations

$$\partial_t f_i + \mathbf{c}_i \cdot \nabla f_i = -\frac{1}{\tau}\left(f_i - f_i^{(0)}\right), \tag{18a}$$

$$\partial_t \mathbf{g}_i + \mathbf{c}_i \cdot \nabla \mathbf{g}_i = -\frac{1}{\tau}\left(\mathbf{g}_i - \mathbf{g}_i^{(0)}\right). \tag{18b}$$

We have used the single-relaxation-time or BGK collision operator with relaxation time $\tau$ on the right-hand sides.[54] Taking the zeroth moments of the two kinetic equations in (18) for suitable choices of equilibrium distribution functions gives the two conservation laws

$$\partial_t \rho + \nabla \cdot \mathbf{J} = 0, \quad \partial_t(\rho \mathbf{u}) + \nabla \cdot \boldsymbol{\Pi} = 0, \tag{19}$$

where the mass flux $\mathbf{J}$ and momentum flux $\boldsymbol{\Pi}$ are defined by

$$\mathbf{J} = \sum_{i=0}^{N-1} \mathbf{c}_i f_i, \quad \boldsymbol{\Pi} = \sum_{i=0}^{N-1} \mathbf{c}_i \mathbf{g}_i. \tag{20}$$

It is necessary to distinguish the mass flux from the momentum density in this vector formulation. The mass flux $\mathbf{J}$ is determined by the first moment of the $f_i$, and the momentum density $\rho\mathbf{u}$ by the zeroth moment of the $\mathbf{g}_i$. We take the equilibrium mass flux to be

$$\mathbf{J}^{(0)} = \sum_{i=0}^{N-1} \mathbf{c}_i f_i^{(0)} = \rho \mathbf{u}. \tag{21}$$

The two vector fields thus coincide at equilibrium, but will not coincide in general.

We take the equilibrium momentum flux to be

$$\boldsymbol{\Pi}^{(0)} = \sum_{i=0}^{N-1} \mathbf{c}_i \mathbf{g}_i^{(0)} = \rho \mathbf{u}\mathbf{u} + \rho I, \tag{22}$$

so the leading-order hydrodynamic equations from (19) are the isothermal compressible Euler equations with unit sound speed

$$\partial_t \rho + \nabla \cdot (\rho \mathbf{u}) = 0, \quad \partial_t(\rho \mathbf{u}) + \nabla \cdot (\rho \mathbf{u}\mathbf{u} + \rho I) = 0. \tag{23}$$

The kinetic formulation is stable with unit sound speed because the particle speed is $\lambda$, which is larger than 2, rather than 1 as in the standard scalar discrete kinetic formulation.

The corresponding equilibrium distributions for the D2Q5 lattice are[23–26]

$$f_0^{(0)} = (1-4a)\rho, \quad \mathbf{g}_0^{(0)} = (1-4a)\rho\mathbf{u}, \tag{24}$$

for the rest particles with $i = 0$, and

$$f_i^{(0)} = a\rho + \frac{1}{2\lambda^2}\mathbf{c}_i \cdot \rho\mathbf{u}, \quad \mathbf{g}_i^{(0)} = a\rho\mathbf{u} + \frac{1}{2\lambda^2}\mathbf{c}_i \cdot \boldsymbol{\Pi}^{(0)}, \tag{25}$$

for the particles with $i \geq 1$. The second constant $a$ must be related to $\lambda$ by the stability condition $2a\lambda > 1$, as described in the Appendix. Each equilibrium distribution is a linear combination of the mass or momentum density, and the inner product of $\boldsymbol{\xi}_i$ with the corresponding mass or momentum flux. The formulation used by Baty *et al.*[25] is equivalent to taking $a = 1/4$ so that $f_0^{(0)}$ and $\mathbf{g}_0^{(0)}$ both vanish. It is then sufficient to use the D2Q4 lattice comprising $\boldsymbol{\xi}_1, \boldsymbol{\xi}_2, \boldsymbol{\xi}_3, \boldsymbol{\xi}_4$ with no rest particles.

### A. Diffusive mass flux

This vector kinetic formulation of hydrodynamics allow density to diffuse, because the mass flux $\mathbf{J}$ computed from the $f_i$ may differ from the momentum density $\rho\mathbf{u}$ computed from the $\mathbf{g}_i$. Taking the $\mathbf{c}_i$ moment of the evolution equation for the $f_i$ gives

$$\partial_t \mathbf{J} + \nabla \cdot \left(\sum_{i=0}^{N-1} \mathbf{c}_i \mathbf{c}_i f_i\right) = -\frac{1}{\tau}(\mathbf{J} - \rho\mathbf{u}). \tag{26}$$

Hydrodynamics is concerned with solutions of the kinetic equations that evolve slowly on timescales much longer than the kinetic relaxation time $\tau$. We seek such solutions by posing a multiple-scales expansion of both the $f_i$ and the time derivative $\partial_t$ as series in $\tau$

$$f_i = f_i^{(0)} + \tau f_i^{(1)} + \cdots, \quad \partial_t = \partial_{t_0} + \tau\partial_{t_1} + \cdots, \tag{27}$$

along with the single solvability condition

$$\sum_{i=0}^{N-1} f_i^{(n)} = 0, \text{ for } n = 1, 2, \ldots. \tag{28}$$

The latter expresses conservation of mass under the relaxation of the $f_i$ toward equilibrium. This is equivalent to expanding $\mathbf{J} = \mathbf{J}^{(0)} + \tau\mathbf{J}^{(1)} + \cdots$ while leaving $\rho$ and $\mathbf{u}$ unexpanded, as in van Kampen's theory for the elimination of fast variables.[55–57]

Substituting these expansions into (26) and truncating at leading order gives

$$\partial_{t_0}\mathbf{J}^{(0)} + \nabla \cdot \left(\sum_{i=0}^{N-1} \mathbf{c}_i \mathbf{c}_i f_i^{(0)}\right) = -\mathbf{J}^{(1)}. \tag{29}$$

Eliminating the leading-order time derivative of $\mathbf{J}^{(0)} = \rho\mathbf{u}$ using the leading-order Euler momentum equation (23) gives

$$\begin{aligned} \mathbf{J}^{(1)} &= -[\partial_{t_0}(\rho\mathbf{u}) + \nabla \cdot (2a\lambda^2 \rho I)], \\ &= -[-\nabla \cdot (\rho\mathbf{u}\mathbf{u} + \rho I) + 2a\lambda^2 \nabla\rho], \\ &= (1 - 2a\lambda^2)\nabla\rho + \nabla \cdot (\rho\mathbf{u}\mathbf{u}). \end{aligned} \tag{30}$$

The density evolution equation to this order,

$$\partial_t \rho + \nabla \cdot \left(\mathbf{J}^{(0)} + \tau\mathbf{J}^{(1)}\right) = 0, \tag{31}$$

thus becomes

$$\partial_t \rho + \nabla \cdot (\rho\mathbf{u}) = \tau\nabla\nabla : \left(((2a\lambda^2 - 1)I - \mathbf{u}\mathbf{u})\rho\right). \tag{32}$$

The : denotes a double tensor contraction, so the last expression is $\partial_\alpha\partial_\beta(\rho u_\alpha u_\beta)$ in index notation. We need $2a\lambda^2 > 1$ to ensure a positive diffusion coefficient for density when the fluid is at rest, and hence a well-posed density evolution equation. This inequality follows

automatically from the existing stability constraints on $a$ and $\lambda$, as described in the Appendix.[23]

### B. Viscous momentum flux

We now apply an equivalent analysis to the evolution equation for the momentum flux

$$\partial_t \mathbf{\Pi} + \nabla \cdot \left( \sum_{i=0}^{N-1} \mathbf{c}_i \mathbf{c}_i \mathbf{g}_i \right) = -\frac{1}{\tau} (\mathbf{\Pi} - \mathbf{\Pi}^{(0)}). \tag{33}$$

We pose a multiple-scales expansion of $\mathbf{\Pi} = \mathbf{\Pi}^{(0)} + \tau \mathbf{\Pi}^{(1)} + \cdots$ and of the time derivative $\partial_t = \partial_{t_0} + \tau \partial_{t_1} + \cdots$ to obtain the leading order equation

$$\partial_{t_0} \mathbf{\Pi}^{(0)} + \nabla \cdot \left( 2a\lambda^2 \rho \mathbf{u} \right) = -\mathbf{\Pi}^{(1)}. \tag{34}$$

The flux in the divergence is the second moment of the $\mathbf{g}_i^{(0)}$

$$\sum_{i=0}^{N-1} \mathbf{c}_i \mathbf{c}_i \mathbf{g}_i^{(0)} = 2a\lambda^2 \rho \mathbf{u}. \tag{35}$$

Calculating the leading-order time derivative of $\mathbf{\Pi}^{(0)}$ from the Euler equations in the usual way gives[58]

$$\begin{aligned} \partial_{t_0} \mathbf{\Pi}^{(0)} &= \partial_{t_0} (\rho \mathbf{u}\mathbf{u} + \rho I), \\ &= \partial_{t_0} (\rho \mathbf{u}) \mathbf{u} + \mathbf{u} \partial_{t_0} (\rho \mathbf{u}) + (I - \mathbf{u}\mathbf{u}) \partial_{t_0} \rho, \\ &= -\nabla \cdot (\rho \mathbf{u}\mathbf{u}) \mathbf{u} - (\nabla \rho) \mathbf{u} - \mathbf{u} \nabla \cdot (\rho \mathbf{u}\mathbf{u}) \\ &\quad - \mathbf{u} (\nabla \rho) - (I - \mathbf{u}\mathbf{u}) \nabla \cdot (\rho \mathbf{u}), \\ &= -\nabla \cdot (\rho \mathbf{u}\mathbf{u}\mathbf{u}) - (\nabla \rho) \mathbf{u} - \mathbf{u} (\nabla \rho) - I \nabla \cdot (\rho \mathbf{u}), \end{aligned} \tag{36}$$

so

$$\begin{aligned} \mathbf{\Pi}^{(1)} = &- 2a\lambda^2 \rho \nabla \mathbf{u} + (1 - 2a\lambda^2)(\nabla \rho)\mathbf{u} + \mathbf{u}(\nabla \rho) \\ &+ I \nabla \cdot (\rho \mathbf{u}) + \nabla \cdot (\rho \mathbf{u}\mathbf{u}\mathbf{u}). \end{aligned} \tag{37}$$

Lattice Boltzmann schemes are commonly used to simulate nearly incompressible flows in which the fluid velocity $\mathbf{u}$ is much smaller than the sound speed $c_s$ so the Mach number $\mathrm{Ma} = |\mathbf{u}|/c_s$ is small. The density is then nearly constant, $\rho = \rho_0 + \delta\rho$ with $\delta\rho/\rho_0 = O(\mathrm{Ma}^2)$. We can thus discard terms involving the density gradient to obtain[23]

$$\tau \mathbf{\Pi}^{(1)} = -2a\lambda^2 \tau \rho \nabla \mathbf{u} + O(\mathrm{Ma}^2). \tag{38}$$

This matches the extended Newtonian constitutive relation in Sec. III with equal shear and vortex viscosities, $\mu_s = \mu_v = a\lambda^2 \tau \rho$, bulk viscosity $\mu_b = (2/D) a\lambda^2 \tau \rho$, but no internal angular velocity. The constitutive relation (38) is thus not invariant under time-dependent rigid rotations. The underlying fixed set of discrete velocities in the kinetic equations defines a preferred orientation. In numerical experiments we will take $\tau \propto 1/\rho$ so that the viscosities are constants, independent of density fluctuations, as assumed in deriving (13). The shear viscosity in a dilute monatomic gas is also independent of density, being a function of temperature only.

Multiparticle collision dynamics,[29–31] also called stochastic rotation dynamics,[32,33] simulates a fluid using particles that may have any location and may move with any velocity. Collisions are modeled by grouping the particles into cells using a Cartesian grid. The particles in each cell have their velocities relative to their center of mass rotated by a random angle. The grid is also translated randomly for each collision to ensure Galilean invariance. The resulting macroscopic stress tensor contains a symmetric shear viscous stress from the particles' motion. There is also a second contribution from the collision model that takes the asymmetric form (38) above.[34,35] This asymmetry causes artifacts in simulations of multiphase flows and flows driven by boundary torques.[36]

## V. DISCRETISATION

We now further discretize in space and time the combined vector discrete Boltzmann system of partial differential equations

$$\partial_t \mathbf{F}_i + \mathbf{c}_i \cdot \nabla \mathbf{F}_i = -\frac{1}{\tau} \left( \mathbf{F}_i - \mathbf{F}_i^{(0)} \right), \tag{39}$$

for the $(D+1)$-dimensional vectors $\mathbf{F}_i = (f_i, \mathbf{g}_i)$. We decompose this equation into its advective and algebraic parts. The exact solution of the advective part over a time step $\Delta t$ can be written using the streaming operator $\mathsf{S}$

$$(\mathsf{S}\mathbf{F})_i(\mathbf{x}, t) = \mathbf{F}_i(\mathbf{x} - \boldsymbol{\xi}_i \Delta x, t - \Delta t). \tag{40}$$

We need to choose the time step $\Delta t = \Delta x/\lambda$ so that $|\mathbf{c}_i| \Delta t = \Delta x$ and $\mathbf{c}_i \Delta t = \boldsymbol{\xi}_i \Delta x$. Any point $\mathbf{x}$ lying in the lattice $\Delta x \mathbb{Z}^D$ moves to another point $\mathbf{x} + \mathbf{c}_i \Delta t$ lying in the same lattice. The time step is thus a factor of $\lambda$ shorter than the time step in a standard lattice Boltzmann formulation using scalar distribution functions.

We approximate the solution of the algebraic part using the Crank–Nicolson discretization

$$\begin{aligned} \frac{\mathbf{F}_i(\mathbf{x}, t + \Delta t) - \mathbf{F}_i(\mathbf{x}, t)}{\Delta t} = &-\frac{1}{2\tau} \Big( \mathbf{F}_i(\mathbf{x}, t + \Delta t) \\ &- \mathbf{F}_i^{(0)}(\mathbf{x}, t + \Delta t) + \mathbf{F}_i(\mathbf{x}, t) - \mathbf{F}_i^{(0)}(\mathbf{x}, t) \Big), \end{aligned} \tag{41}$$

which is second-order accurate in time. The equilibrium $\mathbf{F}_i^{(0)}$ only depends upon the conserved quantities $\rho$ and $\mathbf{u}$, which are unchanged under collisions, so $\mathbf{F}_i^{(0)}(\mathbf{x}, t + \Delta t) = \mathbf{F}_i^{(0)}(\mathbf{x}, t)$. We can thus solve for

$$\mathbf{F}_i(\mathbf{x}, t + \Delta t) = \mathbf{F}_i(\mathbf{x}, t) - \frac{\Delta t}{\tau + \Delta t/2} \left( \mathbf{F}_i(\mathbf{x}, t) - \mathbf{F}_i^{(0)}(\mathbf{x}, t) \right). \tag{42}$$

The right-hand side defines the collision operator $\mathsf{C}$. The Crank–Nicolson discretization leads to the Hénon correction of the relaxation time from $\tau$ in the partial differential equations (39) to $\tau + \Delta t/2$ in the discrete algorithm.[59]

To achieve second-order accuracy, we combine the streaming and collision operators using Strang splitting[60,61]

$$\mathbf{F}(\cdot, t + \Delta t) = \mathsf{C}^{1/2} \mathsf{S} \mathsf{C}^{1/2} \mathbf{F}(\cdot, t), \tag{43}$$

where $\mathbf{F}(\cdot, t)$ denotes all the $\mathbf{F}_i$ at all the grid points at time $t$, and similarly for $\mathbf{F}(\cdot, t + \Delta t)$. The operator $\mathsf{C}^{1/2}$ formally denotes the result of applying the collision operator for a half time step $\Delta t/2$. Applying this Strang splitting over $n$ timesteps and coalescing adjacent pairs of $\mathsf{C}^{1/2}$ operations gives

$$\mathbf{F}(\cdot, t + n\Delta t) = \mathsf{C}^{1/2} (\mathsf{S}\mathsf{C})^n \mathsf{C}^{-1/2} \mathbf{F}(\cdot, t). \tag{44}$$

If we redefine $\mathsf{C}^{1/2} = \frac{1}{2}(\mathsf{I}+\mathsf{C})$ to sufficient accuracy, and $\mathsf{C}^{-1/2} = 2(\mathsf{I}+\mathsf{C})^{-1}$ to be its exact inverse, we recover the variable transformation

$$\overline{\mathbf{F}}(\cdot,t) = \mathsf{C}^{-1/2}\mathbf{F}(\cdot,t) \tag{45}$$

introduced by He *et al.*[62] for the single-relaxation-time collision operator. The numerical algorithm then becomes the familiar lattice Boltzmann stream/collide sequence applied to the transformed variables:

$$\overline{\mathbf{F}}(\cdot,t+n\Delta t) = (SC)^n\overline{\mathbf{F}}(\cdot,t). \tag{46}$$

We use the Crank–Nicolson method (41) rather than the available exact solution for the collision step because the lattice Boltzmann approach relies upon a cancelation between the Strang splitting error and the Crank–Nicolson discretization error when $\tau < \Delta t$. Such small $\tau$ values are needed to achieve grid-scale Reynolds numbers above unity.[61,63]

This numerical algorithm operates on the transformed variables $\overline{\mathbf{F}}_i$. To recover the momentum flux $\boldsymbol{\Pi}$, we first compute the transformed momentum flux

$$\overline{\boldsymbol{\Pi}} = \sum_{i=0}^{N-1}\boldsymbol{\xi}_i\overline{\mathbf{g}}_i. \tag{47}$$

We then apply the operator $\frac{1}{2}(\mathsf{I}+\mathsf{C})$ to form

$$\boldsymbol{\Pi} = \frac{1}{2}(\mathsf{I}+\mathsf{C})\overline{\boldsymbol{\Pi}} = \frac{1}{2}\left(\overline{\boldsymbol{\Pi}}+\overline{\boldsymbol{\Pi}}'\right) = \frac{\overline{\boldsymbol{\Pi}}\tau+\boldsymbol{\Pi}^{(0)}\Delta t/2}{\tau+\Delta t/2}. \tag{48}$$

We can interpret $\boldsymbol{\Pi}$ as the average of the pre-collisional momentum flux $\overline{\boldsymbol{\Pi}}$ and the post-collisional momentum flux $\overline{\boldsymbol{\Pi}}' = \mathsf{C}\,\overline{\boldsymbol{\Pi}}$.

## VI. COLLISION OPERATOR WITH ADJUSTABLE VORTEX VISCOSITY

The previous discretization was constructed using the BGK collision operator. We can change the collision operator to apply different relaxation rates to the symmetric and antisymmetric parts of the momentum flux. This follows earlier work to adjust the relaxation rate for the antisymmetric part of the electric field tensor in lattice Boltzmann formulations of magnetohydrodynamics.[19,20]

We want to recover a constitutive relation with a vortex viscosity, as in Sec. III, but with $\mathbf{s} = 0$, and with $\mu_b = 2\mu_s/D$ as usual for a lattice Boltzmann formulation of an isothermal fluid in which collisions conserve temperature rather than energy. The momentum flux should be

$$\boldsymbol{\Pi} = \boldsymbol{\Pi}^{(0)} - \mu_s\left(\nabla\mathbf{u}+(\nabla\mathbf{u})^{\mathsf{T}}\right) - \mu_\nu\left(\nabla\mathbf{u}-(\nabla\mathbf{u})^{\mathsf{T}}\right), \tag{49}$$

to the first two orders in a Chapman–Enskog expansion. We can achieve this by adapting (33) and (34) for a collision operator that applies different relaxation times $\tau_S$ and $\tau_A$ to the symmetric and antisymmetric parts of $\boldsymbol{\Pi}$. Equation (33) then becomes

$$\partial_t\boldsymbol{\Pi} + \nabla\cdot\left(\sum_{i=0}^{N-1}\mathbf{c}_i\mathbf{c}_i\mathbf{g}_i\right) = -\frac{1}{\tau_S}[\boldsymbol{\Pi}-\boldsymbol{\Pi}^{(0)}]_S - \frac{1}{\tau_A}[\boldsymbol{\Pi}-\boldsymbol{\Pi}^{(0)}]_A. \tag{50}$$

We have written the symmetric and antisymmetric parts of a tensor $\boldsymbol{\Pi}$ as

$$[\boldsymbol{\Pi}]_S = \frac{1}{2}(\boldsymbol{\Pi}+\boldsymbol{\Pi}^{\mathsf{T}}), \quad [\boldsymbol{\Pi}]_A = \frac{1}{2}(\boldsymbol{\Pi}-\boldsymbol{\Pi}^{\mathsf{T}}). \tag{51}$$

The Chapman–Enskog solution of (50) is (49) with $\mu_s = a\lambda^2\rho\tau_S$ and $\mu_\nu = a\lambda^2\rho\tau_A$ at leading order in Mach number. We recover the previous case when $\tau_S = \tau_A$.

Applying the Crank–Nicolson discretization to the right-hand side of (50) as part of the Strang splitting procedure from Sec. V gives the post-collisional momentum flux

$$\overline{\boldsymbol{\Pi}}' = \overline{\boldsymbol{\Pi}} - \frac{\Delta t}{\tau_S+\Delta t/2}[\overline{\boldsymbol{\Pi}}-\boldsymbol{\Pi}^{(0)}]_S - \frac{\Delta t}{\tau_A+\Delta t/2}[\overline{\boldsymbol{\Pi}}]_A, \tag{52}$$

using the symmetry of $\boldsymbol{\Pi}^{(0)}$. We can rewrite this as

$$\overline{\boldsymbol{\Pi}}' = \boldsymbol{\Pi}^{(0)} + \frac{\tau_S-\Delta t/2}{\tau_S+\Delta t/2}[\overline{\boldsymbol{\Pi}}-\boldsymbol{\Pi}^{(0)}]_S + \frac{\tau_A-\Delta t/2}{\tau_A+\Delta t/2}[\overline{\boldsymbol{\Pi}}]_A. \tag{53}$$

The coefficient of the antisymmetric term remains finite even if we set $\tau_A = 0$, since $\tau_A + \Delta t/2$ appears in the denominator according to the Hénon correction.[59] Setting $\tau_A = 0$ sets the coefficient of $[\overline{\boldsymbol{\Pi}}]_A$ to minus one, so the antisymmetric part of $\overline{\boldsymbol{\Pi}}$ reverses its sign during the collision step. If we wanted the post-collisional momentum flux to be symmetric we would need $\tau_A = \Delta t/2$. This corresponds to a fairly large vortex viscosity, typically much larger than the shear viscosity.

The collision step with $\tau_A = 0$ is on the boundary for linear stability. The equivalent zero relaxation time limit has been used successfully elsewhere to simulate non-dissipative electromagnetic wave propagation,[16,18] and in palindromic relaxation schemes for hyperbolic systems.[37]

We can also rewrite (52) as

$$\overline{\boldsymbol{\Pi}}' = \overline{\boldsymbol{\Pi}} - \frac{\Delta t}{\tau_S+\Delta t/2}(\overline{\boldsymbol{\Pi}}-\boldsymbol{\Pi}^{(0)}) + \frac{1}{2}(\tau_A-\tau_S)\frac{\Delta t}{(\tau_S+\Delta t/2)(\tau_A+\Delta t/2)}(\overline{\boldsymbol{\Pi}}-\overline{\boldsymbol{\Pi}}^{\mathsf{T}}). \tag{54}$$

The first two terms now match those arising from the usual single relaxation time collision operation. When $\tau_A = 0$ this further simplifies to

$$\overline{\boldsymbol{\Pi}}' = \overline{\boldsymbol{\Pi}} - \frac{\Delta t}{\tau_S+\Delta t/2}(\overline{\boldsymbol{\Pi}}-\boldsymbol{\Pi}^{(0)}) - \frac{\tau_S}{\tau_S+\Delta t/2}(\overline{\boldsymbol{\Pi}}-\overline{\boldsymbol{\Pi}}^{\mathsf{T}}). \tag{55}$$

This collision operator is most easily implemented by applying the BGK collision operator to the distribution functions, then adding the rightmost term proportional to $\overline{\boldsymbol{\Pi}}-\overline{\boldsymbol{\Pi}}^{\mathsf{T}}$ from (54) or (55) to adjust the antisymmetric part of $\overline{\boldsymbol{\Pi}}'$. The post-collisional distribution functions in two dimensions are

$$\overline{g}'_{ix} = \overline{g}_{ix} - \frac{\Delta t}{\tau_S+\Delta t/2}\left(\overline{g}_{ix}-\overline{g}^{(0)}_{ix}\right) - \frac{1}{2\lambda}\xi_{iy}\Delta\Pi, \tag{56a}$$

$$\overline{g}'_{iy} = \overline{g}_{iy} - \frac{\Delta t}{\tau_S+\Delta t/2}\left(\overline{g}_{iy}-\overline{g}^{(0)}_{iy}\right) + \frac{1}{2\lambda}\xi_{ix}\Delta\Pi, \tag{56b}$$

with a correction proportional to

$$\Delta\Pi = \frac{1}{2}(\tau_A-\tau_S)\frac{\Delta t}{(\tau_S+\Delta t/2)(\tau_A+\Delta t/2)}\left(\overline{\Pi}_{xy}-\overline{\Pi}_{yx}\right). \tag{57}$$

For $\tau_A = 0$ this correction simplifies to

$$\Delta\Pi = -\frac{\tau_S}{(\tau_S + \Delta t/2)}\left(\overline{\Pi}_{xy} - \overline{\Pi}_{yx}\right). \tag{58}$$

### A. Analysis of the discretization in the $\tau_A \to 0$ limit

To analyze the behavior of the collision operator as we take $\tau_A \to 0$, or even set $\tau_A = 0$, we consider an evolution equation for the momentum flux of the form

$$\partial_t \mathbf{\Pi} + \nabla \cdot \mathbf{Q} = -\mathbf{\Omega}(\mathbf{\Pi} - \mathbf{\Pi}^{(0)}), \tag{59}$$

where $\mathbf{\Omega}$ is a constant linear operator that maps rank-2 tensors to rank-2 tensors. For example, the BGK collision operator corresponds to $\mathbf{\Omega} = (1/\tau)\mathbf{1}$, with $\mathbf{1}$ the identity operator that acts on rank-2 tensors. One can think of $\mathbf{\Pi}$ as a column vector with $D^2$ components, for example, as $(\Pi_{xx}, \Pi_{xy}, \Pi_{yx}, \Pi_{yy})^{\mathsf{T}}$ in two dimensions, and $\mathbf{\Omega}$ as a $D^2 \times D^2$ matrix.

The Crank–Nicolson discretization of the collision step to solve

$$\partial_t \mathbf{\Pi} = -\mathbf{\Omega}(\mathbf{\Pi} - \mathbf{\Pi}^{(0)}), \tag{60}$$

over a time step $\Delta t$ defines the discrete collision operator

$$\mathscr{C} = \left(\mathbf{1} - \frac{1}{2}\Delta t\mathbf{\Omega}\right)\left(\mathbf{1} + \frac{1}{2}\Delta t\mathbf{\Omega}\right)^{-1} \tag{61}$$

to be the Cayley transform of $\frac{1}{2}\Delta t\mathbf{\Omega}$. Its expansion

$$\mathscr{C} = \mathbf{1} - \Delta t\mathbf{\Omega} + \frac{1}{2}\Delta t^2\mathbf{\Omega}^2 + O(\Delta t^3||\mathbf{\Omega}||^3) \tag{62}$$

matches the first three terms in the expansion of $\exp(-\Delta t\mathbf{\Omega})$ for small $\Delta t$. If we treat $\mathbf{\Omega}$ and $\mathscr{C}$ as matrices, $\mathscr{C}$ has the same eigenvectors as $\mathbf{\Omega}$. Eigenvalues of $\mathbf{\Omega}$ in the range $[0, \infty)$ map to eigenvalues of $\mathscr{C}$ in the range $(-1, 1]$. In particular, an eigenvalue of $\mathbf{\Omega}$ that tends to infinity maps to an eigenvalue of $\mathscr{C}$ that tends to $-1$, a finite limiting value. The discrete collision operator is thus well defined even when $\mathbf{\Omega}$ has an infinite eigenvalue, or equivalently a zero relaxation time. This follows from replacing (59) with

$$\mathbf{\Omega}^{\text{inv}}(\partial_t \mathbf{\Pi} + \nabla \cdot \mathbf{Q}) = -(\mathbf{\Pi} - \mathbf{\Pi}^{(0)}). \tag{63}$$

This is equivalent to (59) when $\mathbf{\Omega}$ is an invertible matrix, as seen by taking $\mathbf{\Omega}^{\text{inv}} = \mathbf{\Omega}^{-1}$, but (63) remains valid when $\mathbf{\Omega}^{\text{inv}}$ has a zero eigenvalue. The Cayley transform becomes

$$\mathscr{C} = \left(\mathbf{\Omega}^{\text{inv}} - \frac{1}{2}\Delta t\mathbf{1}\right)\left(\mathbf{\Omega}^{\text{inv}} + \frac{1}{2}\Delta t\mathbf{1}\right)^{-1}. \tag{64}$$

In particular, we can take $\mathbf{\Omega}^{\text{inv}} = \tau\mathscr{P}$, a scalar multiple of the projection operator $\mathscr{P}$ that projects the left-hand side of (59) onto the space of symmetric tensors (see Sec. VII).

### B. Local calculation of the vorticity

The post-collisional momentum flux $\overline{\mathbf{\Pi}}'$ is related to the pre-collisional momentum flux $\overline{\mathbf{\Pi}}$ by

$$\overline{\mathbf{\Pi}}' = \mathbf{\Pi}^{(0)} + \mathscr{C}(\overline{\mathbf{\Pi}} - \mathbf{\Pi}^{(0)}), \tag{65}$$

where the transformed momentum flux is

$$\overline{\mathbf{\Pi}} = \mathbf{\Pi}^{(0)} + \left(\mathbf{1} + \frac{1}{2}\Delta t\mathbf{\Omega}\right)(\mathbf{\Pi} - \mathbf{\Pi}^{(0)}). \tag{66}$$

We can therefore express the right-hand side of (59) as

$$-\mathbf{\Omega}(\mathbf{\Pi} - \mathbf{\Pi}^{(0)}) = (1/\Delta t)(\overline{\mathbf{\Pi}}' - \overline{\mathbf{\Pi}}). \tag{67}$$

The multiple-scales expansion leads to

$$\begin{aligned}(1/\Delta t)(\overline{\mathbf{\Pi}}' - \overline{\mathbf{\Pi}}) &= -\mathbf{\Omega}(\mathbf{\Pi} - \mathbf{\Pi}^{(0)}) \\ &= \partial_{t_0}\mathbf{\Pi}^{(0)} + \nabla \cdot \mathbf{Q}^{(0)} = 2a\lambda^2\rho\nabla\mathbf{u} + \cdots,\end{aligned} \tag{68}$$

so we can recover a consistent approximation of the velocity gradient from $\mathscr{C}$ and $\overline{\mathbf{\Pi}}$ using

$$\nabla\mathbf{u} = \frac{1}{2a\lambda^2\rho\Delta t}(\mathscr{C} - \mathbf{1})\overline{\mathbf{\Pi}}. \tag{69}$$

The objects $\mathscr{C}$ and $\overline{\mathbf{\Pi}}$ remain well behaved when one or more of the relaxation times in $\mathbf{\Omega}$ is set to zero, We can use this relation to diagnose the vorticity $\boldsymbol{\omega} = \nabla \times \mathbf{u} = \boldsymbol{\epsilon} : (\nabla\mathbf{u})$ locally at lattice points. For example, the vorticity in two dimensions is

$$\omega = \frac{\overline{\Pi}'_{xy} - \overline{\Pi}_{xy} - (\overline{\Pi}'_{yx} - \overline{\Pi}_{yx})}{2a\lambda^2\rho\Delta t}. \tag{70}$$

This is how the electric current $\nabla \times \mathbf{B}$ can be locally computed in lattice Boltzmann algorithms for magnetohydrodynamics that use vector distribution functions to represent the magnetic field.[17,19] However, it has not previously been applied when the relaxation time for the antisymmetric part of the relevant tensor has been set to zero.

It is not possible to locally compute the vorticity from the distribution functions in conventional hydrodynamic lattice Boltzmann algorithms using scalar distribution functions since $\mathbf{\Pi}$ is symmetric. One can only compute the symmetric strain rate tensor $\frac{1}{2}(\nabla\mathbf{u} + \nabla\mathbf{u}^{\mathsf{T}})$ from $\mathbf{\Pi} - \mathbf{\Pi}^{(0)}$. This is used in many lattice Boltzmann formulations of generalized Newtonian fluids with strain-rate dependent viscosities,[64–66] and the Smagorinski turbulence model.[67–69]

### C. Consistent initialization

It is common to initialize a lattice Boltzmann simulation by setting the distribution functions to their equilibrium values for the initial fluid velocity field and a uniform density. However, this excites sound waves because the initial pressure field is not compatible with the velocity field. It also excites oscillations in the momentum flux because the viscous stress is set to zero initially. The initial viscous torque will therefore also be zero. To do better, we follow Skordos[70] by initializing the density and the non-equilibrium part of the momentum flux consistently with the initial velocity field.

The pressure in an incompressible flow with constant density $\rho_0$ is determined by the divergence of the momentum evolution equation

$$0 = \rho_0\partial_t\nabla \cdot \mathbf{u} = -\nabla\nabla : (p\mathsf{I} + \rho_0\mathbf{uu}). \tag{71}$$

The pressure in a fluid with an isothermal equation of state is $p = c_s^2\rho$, and $\rho = \rho_0 + \delta\rho$ with $\delta\rho/\rho_0 = O(\text{Ma}^2)$ in a low Mach number flow. Equation (71) thus becomes

$$c_s^2\nabla^2\delta\rho + \rho_0\nabla\nabla : (\mathbf{uu}) = 0, \tag{72}$$

at leading order in Mach number. This also confirms the scaling $\delta\rho/\rho_0 \sim |\mathbf{u}|^2/c_s^2$. We can solve this Poisson equation for $\delta\rho$ either analytically, or using discrete Fourier transforms in a domain with periodic boundary conditions.

Turning to the viscous stress, (68) can be rewritten as

$$(\mathbf{1}-\mathscr{C})(\overline{\mathbf{\Pi}}-\mathbf{\Pi}^{(0)}) = -2a\lambda^2\rho\Delta t\nabla\mathbf{u}+\cdots, \tag{73}$$

so we can construct a consistent initial momentum flux using

$$\overline{\mathbf{\Pi}} = \mathbf{\Pi}^{(0)} - 2a\lambda^2\rho\Delta t(\mathbf{1}-\mathscr{C})^{-1}\nabla\mathbf{u}. \tag{74}$$

The operator $\Delta t(\mathbf{1}-\mathscr{C})^{-1} = \mathbf{\Omega}^{-1}+\frac{1}{2}\Delta t\mathbf{1}$ has a well-defined limit even if one or more of the relaxation times in $\mathbf{\Omega}$ is set to zero. For the BGK collision operator, we get

$$\overline{\mathbf{\Pi}} = \mathbf{\Pi}^{(0)} - 2a\lambda^2\rho\left(\tau+\frac{1}{2}\Delta t\right)\nabla\mathbf{u}. \tag{75}$$

For the collision operator with adjustable vortex viscosity, we get

$$\overline{\mathbf{\Pi}} = \mathbf{\Pi}^{(0)} - a\lambda^2\rho\left\{\left(\tau_S+\frac{1}{2}\Delta t\right)(\nabla\mathbf{u}+\nabla\mathbf{u}^{\mathsf{T}}) + \left(\tau_A+\frac{1}{2}\Delta t\right)(\nabla\mathbf{u}-\nabla\mathbf{u}^{\mathsf{T}})\right\}, \tag{76}$$

which simplifies to

$$\overline{\mathbf{\Pi}} = \mathbf{\Pi}^{(0)} - a\lambda^2\rho\left\{(\tau_S+\tau_A+\Delta t)\nabla\mathbf{u}+(\tau_S-\tau_A)\nabla\mathbf{u}^{\mathsf{T}}\right\}. \tag{77}$$

This is perfectly well behaved when $\tau_A = 0$. As in Sec. IV B, we take the relaxation coefficients $\tau_S$ and $\tau_A$ to be proportional to $1/\rho$. The dynamic viscosities $\mu_s = a\lambda^2\rho\tau_S$ and $\mu_v = a\lambda^2\rho\tau_A$ are then constants, so

$$\overline{\mathbf{\Pi}} = \mathbf{\Pi}^{(0)} - \left\{(\mu_s+\mu_v+a\lambda^2\rho\Delta t)\nabla\mathbf{u}+(\mu_s-\mu_v)\nabla\mathbf{u}^{\mathsf{T}}\right\}. \tag{78}$$

We only need the consistent initial density field to calculate the $\rho\Delta t\nabla\mathbf{u}$ contribution.

## VII. THE DISCRETE COLLISION OPERATOR AS A PROJECTION ONTO SYMMETRIC TENSORS

Another way to explore the $\tau_A \to 0$ limit is to consider an evolution equation for $\mathbf{\Pi}$ that involves a projection onto the space of symmetric tensors. There is a close analogy with the Chorin–Temam projection scheme for the incompressible Navier–Stokes equations.[38,39] We write this scheme as

$$\partial_t\mathbf{u} + (\mathbf{u}\cdot\nabla\mathbf{u}+\nabla p) = \nu\nabla^2\mathbf{u}, \tag{79}$$

for a fluid with unit density and kinematic viscosity $\nu$. We interpret the grouping $(\mathbf{u}\cdot\nabla\mathbf{u}+\nabla p)$ as the orthogonal projection of $\mathbf{u}\cdot\nabla\mathbf{u}$ onto the space of divergence-free vector fields. Taking the divergence of (79) gives a Poisson equation

$$\nabla\cdot(\mathbf{u}\cdot\nabla\mathbf{u})+\nabla^2 p = 0 \tag{80}$$

that determines $p$ given suitable boundary conditions. However, choosing such boundary conditions is the main obstacle to implementing these projection schemes in practice.[71] One normally wants boundary conditions on the velocity, not on the pressure.

The Chorin–Temam projection scheme approximates the solution of (79) over discrete time steps $\mathbf{u}^0, \mathbf{u}^1, \ldots$ by constructing an intermediate state

$$\mathbf{u}^\star = \mathbf{u}^n + \Delta t(-\mathbf{u}^n\cdot\nabla\mathbf{u}^n+\nu\nabla^2\mathbf{u}^n), \tag{81}$$

using every term except the pressure, then projecting $\mathbf{u}^\star$ onto the space of divergence-free vector fields to form

$$\mathbf{u}^{n+1} = \mathbf{u}^\star - \Delta t\nabla p^{n+1}. \tag{82}$$

The pressure $p^{n+1}$ solves

$$\nabla^2 p^{n+1} = (1/\Delta t)\nabla\cdot\mathbf{u}^\star. \tag{83}$$

The solution $\mathbf{u}^{n+1}$ at the next time step satisfies $\nabla\cdot\mathbf{u}^{n+1} = 0$ exactly, both when $\mathbf{x}$ is continuous, and when $\mathbf{x}$ is discretized using a consistent discretization of the divergence, gradient and Laplacian operators for which the vector identity $\nabla^2 p = \nabla\cdot(\nabla p)$ still holds discretely.

Returning to our vector kinetic scheme for hydrodynamics, we would like to write the evolution equation for $\mathbf{\Pi}$ in the form

$$\mathscr{P}(\partial_t\mathbf{\Pi}+\nabla\cdot\mathbf{Q}) = -\frac{1}{\tau}(\mathbf{\Pi}-\mathbf{\Pi}^{(0)}), \tag{84}$$

where $\mathscr{P}$ denotes a projection onto symmetric tensors, so $\mathscr{P}\mathbf{A} = \frac{1}{2}(\mathbf{A}+\mathbf{A}^{\mathsf{T}})$ for any tensor $\mathbf{A}$. The multiple-scales expansion of the solution of (84) then gives

$$\mathbf{\Pi}^{(1)} = -\tau\mathscr{P}\left(\partial_{t_0}\mathbf{\Pi}^{(0)}+\nabla\cdot\mathbf{Q}^{(0)}\right). \tag{85}$$

We thus have a symmetric first correction $\mathbf{\Pi}^{(1)}$ and hence a symmetric viscous stress. In principle, we can move the projection operator in (84) to act only on the $\nabla\cdot\mathbf{Q}$ term, since $\partial_{t_0}\mathbf{\Pi}^{(0)}$ is automatically symmetric. However, the analogous result does not hold if we discretize (84) using operator splitting with discrete time steps. The streaming step will create an asymmetric $\mathbf{\Pi}$ that needs to be symmetrized in the collision step.

Equation (84) only determines the symmetric part of $\partial_t\mathbf{\Pi}$, so we cannot solve (84) for $\partial_t\mathbf{\Pi}$. We thus replace (84) with

$$\partial_t\mathbf{\Pi}+\nabla\cdot\mathbf{Q} = -\frac{1}{\tau}(\mathbf{\Pi}-\mathbf{\Pi}^{(0)})+\boldsymbol{\epsilon}\cdot\boldsymbol{\lambda}, \tag{86}$$

where $\boldsymbol{\epsilon}\cdot\boldsymbol{\lambda}$ is a general antisymmetric tensor field expressed using a vector field $\boldsymbol{\lambda}$ of Lagrange multipliers. Taking the antisymmetric part of (86) gives

$$\frac{1}{2}\boldsymbol{\epsilon}:(\nabla\cdot\mathbf{Q}) = \boldsymbol{\lambda}, \tag{87}$$

the analog of (80) that determines the pressure $p$ in the Chorin–Temam projection scheme. However, (87) is just an algebraic equation for $\boldsymbol{\lambda}$ that does not require any boundary conditions.

To implement this projection approach in the lattice Boltzmann collision step, we construct an intermediate state

$$\overline{\mathbf{\Pi}}^\star = \mathbf{\Pi}^{(0)}+\mathscr{C}(\overline{\mathbf{\Pi}}-\mathbf{\Pi}^{(0)}), \tag{88}$$

where $\mathscr{C}$ is the Cayley transform of some continuous collision operator, and a family of post-collisional momentum fluxes

$$\overline{\mathbf{\Pi}}^{\text{post}} = \overline{\mathbf{\Pi}}^\star+\boldsymbol{\epsilon}\cdot\boldsymbol{\lambda} \tag{89}$$

parametrized by a vector Lagrange multiplier $\boldsymbol{\lambda}$. Given the variable transformation from $\mathbf{g}_i$ to $\bar{\mathbf{g}}_i$ we want $\boldsymbol{\Pi} = \frac{1}{2}(\overline{\boldsymbol{\Pi}} + \overline{\boldsymbol{\Pi}}^{\text{post}})$ to be symmetric, not $\overline{\boldsymbol{\Pi}}^{\text{post}}$ itself, so we choose the Lagrange multiplier

$$\boldsymbol{\lambda} = -\frac{1}{2}\boldsymbol{\epsilon} : \left(\overline{\boldsymbol{\Pi}} + \overline{\boldsymbol{\Pi}}^{\text{post}}\right) = -\frac{1}{2}\boldsymbol{\epsilon} : (\mathbf{1} + \mathscr{C})(\overline{\boldsymbol{\Pi}} - \boldsymbol{\Pi}^{(0)}). \tag{90}$$

The post-collisional distribution is then

$$\overline{\boldsymbol{\Pi}}^{\text{post}} = \boldsymbol{\Pi}^{(0)} + \left(\mathscr{C} - \frac{1}{2}\boldsymbol{\epsilon}\cdot\boldsymbol{\epsilon} : (\mathbf{1} + \mathscr{C})\right)(\overline{\boldsymbol{\Pi}} - \boldsymbol{\Pi}^{(0)}). \tag{91}$$

The $\boldsymbol{\epsilon}$ part is antisymmetric, so the symmetric and antisymmetric parts of this equation take their expected forms

$$\left[\overline{\boldsymbol{\Pi}}^{\text{post}}\right]_S = \boldsymbol{\Pi}^{(0)} + \mathscr{C}\left([\overline{\boldsymbol{\Pi}}]_S - \boldsymbol{\Pi}^{(0)}\right), \tag{92a}$$

$$\left[\overline{\boldsymbol{\Pi}}^{\text{post}}\right]_A = -[\overline{\boldsymbol{\Pi}}]_A. \tag{92b}$$

## VIII. NUMERICAL EXPERIMENTS

We consider two sets of two-dimensional numerical experiments to show that the vector lattice Boltzmann scheme with the BGK collision operator satisfies the extended angular momentum evolution equation (8) with an additional $\boldsymbol{\epsilon} : \boldsymbol{\Pi}$ source term, while the projection scheme with zero vortex viscosity satisfies the usual angular momentum conservation law (9). Our aim is to construct reasonable second-order accurate discrete approximations to the surface and line integrals using values of the hydrodynamic variables at lattice points. The first set of numerical experiments uses the Taylor–Green vortex to test solely the viscous part of the torque. The second set uses the Minion–Brown roll-up problem to also test the advective part of the torque.

Both sets of numerical experiments use the domain $(x, y) \in [0, 1]^2$ with periodic boundary conditions. The edges and vertices of the bottom-left quadrant $(x, y) \in [0, 1/2]^2$ lie on lattice points when we use an even number of points. We approximate the area integral using the two-dimensional trapezoidal rule with relative weights 1 for interior points, $1/2$ for most edge points, and $1/4$ for the four vertices, as shown in Fig. 1. We treat each lattice point as representing its Voroni cell, the set of points closer to this lattice point than to any other lattice point.[72] The integration region contains the whole Voroni cell of each interior point, but only half of the Voroni cells of the edge points, and a quarter of the Voroni cells of the four vertices. Similarly, we approximate the line integral around the boundary using relative weights of 1 for points on the straight edges, and weights of $1/2$ for the four vertices, as shown in Fig. 1.

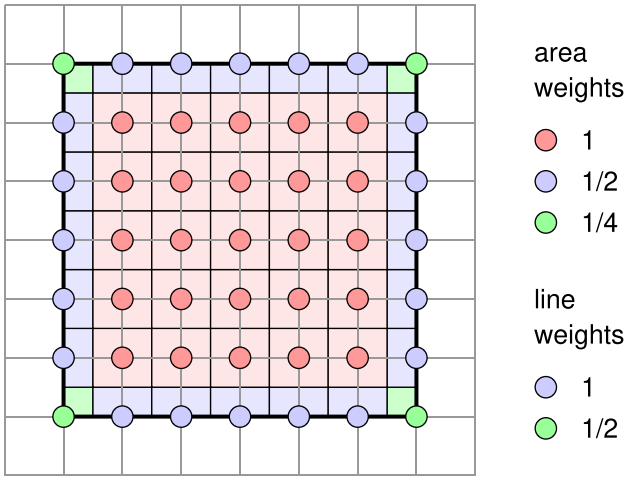


**FIG. 1.** Weights for the discrete area and line integrals over the interior, edges, and corners of a square region.

We define a discrete angular momentum

$$L(t) = \Delta x^2 \sum_{\mathbf{x}} W^{(A)}(\mathbf{x})\,(\mathbf{x} \times \rho\mathbf{u}) \cdot \hat{\mathbf{z}}, \\ = \Delta x^2 \sum_{\mathbf{x}} W^{(A)}(\mathbf{x})\,(xu_y - yu_x)\rho, \tag{93}$$

where $\hat{\mathbf{z}}$ is a unit vector in the $z$ direction, and a discrete interior torque

$$T_{\text{int}}(t) = \Delta x^2 \sum_{\mathbf{x}} W^{(A)}(\mathbf{x})\,\boldsymbol{\epsilon} : \boldsymbol{\Pi} \cdot \hat{\mathbf{z}}, \tag{94}$$

using the area weights $W^{(A)}$. We also define a discrete boundary torque

$$T_{\text{bndry}}(t) = \Delta x \sum_{\mathbf{x}} W^{(L)}(\mathbf{x})\,\mathbf{n} \cdot (\boldsymbol{\Pi} \times \mathbf{x}) \cdot \hat{\mathbf{z}}, \tag{95}$$

using the line weights $W^{(L)}$. The vector expression in the sum evaluates to $\mathbf{n} \cdot (\boldsymbol{\Pi} \times \mathbf{x}) \cdot \hat{\mathbf{z}} = y\Pi_{xx} - x\Pi_{xy}$ on the right boundary of the integration region, and $\mathbf{n} \cdot (\boldsymbol{\Pi} \times \mathbf{x}) \cdot \hat{\mathbf{z}} = y\Pi_{yx} - x\Pi_{yy}$ on the top boundary. These formulas hold with the opposite signs on the left and bottom boundaries with $\mathbf{n}$ reversed in direction.

We then define a total torque $T = T_{\text{bndry}} + T_{\text{int}}$ and an approximate angular momentum

$$\hat{L}(n\Delta t) = L(0) + \Delta t \sum_{r=0}^{n-1} \frac{1}{2}(T(r\Delta t) + T((r+1)\Delta t)), \\ = L(0) + \Delta t\left(\frac{1}{2}T(0) + \sum_{r=1}^{n-1} T(r\Delta t) + \frac{1}{2}T(n\Delta t)\right). \tag{96}$$

This is equal to the initial angular momentum $L(0)$ at $t = 0$ plus a sum of discrete torques. This particular discrete approximation arises from solving $\mathrm{d}L/\mathrm{d}t = T$ using the Crank–Nicolson discretization, or equivalently from approximating $\int_0^t T(t')\mathrm{d}t'$ using the trapezium rule. We will confirm later that $\hat{L}$ and $L$ agree to second-order accuracy in $\Delta t$ in numerical experiments.

### A. Taylor–Green vortex

We first consider the two-dimensional Taylor–Green[73] vortex with velocity field

$$u_x = \sin(2\pi x)\cos(2\pi y)\exp(-8\pi^2\nu t), \\ u_y = -\cos(2\pi x)\sin(2\pi y)\exp(-8\pi^2\nu t), \tag{97}$$

in the domain $(x, y) \in [0, 1]^2$ with periodic boundary conditions. The nonlinear $\mathbf{u} \cdot \nabla\mathbf{u}$ term in the Navier–Stokes equation is exactly balanced by the pressure gradient, so the flow decays linearly like $\exp(-8\pi^2\nu t)$ with an unchanging spatial structure.[74] The dimensionless initial density field that ensures $\nabla\nabla : \boldsymbol{\Pi}^{(0)} = 0$ for an initially non-divergent fluid flow is

$$\rho = 1 + \frac{1}{4}\mathrm{Ma}^2\left(\cos(4\pi x) + \cos(4\pi y)\right), \tag{98}$$

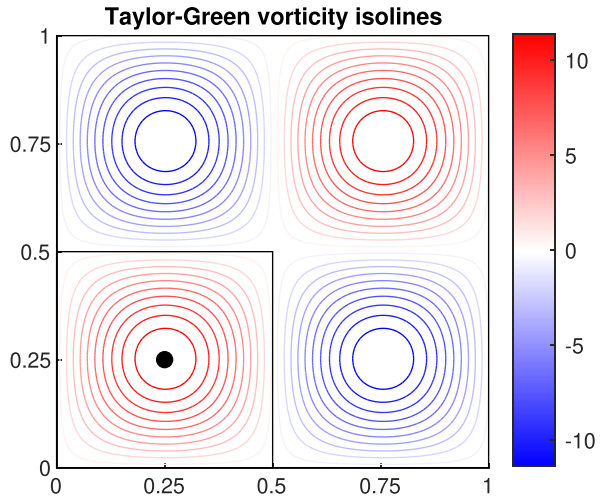


**FIG. 2.** Vorticity field of the Taylor–Green vortex with the bottom-left quadrant highlighted.

to leading order in Mach number.

Figure 2 shows the initial vorticity field for the Taylor–Green vortex, and highlights the bottom-left quadrant with $(x, y) \in [0, 1/2]^2$. The fluid in this quadrant has angular momentum $1/\pi^3$ about the point $(1/4, 1/4)$ at $t = 0$. The corresponding integrated torque on the boundary of this quadrant is $-8\nu/\pi$ at $t = 0$, as it must be, to give the $\exp(-8\pi^2\nu t)$ exponential decay. The torque is purely viscous as the boundary of the quadrant lies on a streamline. There is no advective flux of angular momentum into or out of the quadrant.

Figure 3 shows the evolution of the total angular momentum $L(t)$ in the bottom-left quadrant over time for a numerical experiment using the vector formulation with the BGK collision operator on a $128 \times 128$ lattice with kinematic viscosity $\nu = 0.01$ and Mach number $\mathrm{Ma} = 1/128$. The evolution is a good visual match with the exact solution, and with the integrated torque $\hat{L}(t)$ calculated using the boundary torque and the interior torque together. The corresponding integral of just the boundary torque decays at only half the expected rate. For this flow, the boundary torque and the interior torque are both equal to half the Navier–Stokes boundary torque. It is necessary to include both torques to obtain the correct evolution equation for angular momentum. Figure 4 shows the two torques at early times. The boundary torque shows resolved acoustic oscillations, but the interior torque due to $\boldsymbol{\epsilon} : \boldsymbol{\Pi}$ does not. The consistent initialization from Sec. VI C that includes the viscous $\nabla \mathbf{u}$ terms in $\overline{\boldsymbol{\Pi}}$ has almost completely suppressed any initial zig–zag oscillations from time step to time step.

Figures 5 and 6 show the corresponding data for the symmetrized scheme using the collision operator from Sec. VI with $\tau_A = 0$. The evolution of the angular momentum is now consistent with just the boundary torque. The interior torque is no longer required. The consistent initialization again almost completely suppresses zig–zag oscillations from time step to time step in the boundary torque. Figure 7 shows that $L(n\Delta t) = \hat{L}(n\Delta t) + O(1/N^2)$ on an $N \times N$ lattice. The angular momentum conservation law with the boundary torque alone is satisfied to second-order accuracy in $\Delta x = 1/N$ at fixed Mach number.

### B. Doubly periodic shear layers

For our second set of numerical experiments, we employ the initial conditions used by Bell *et al.*[75] and Minion and Brown[76]

$$u_x = \begin{cases} \tanh(\kappa(y - 1/4)), & y \le 1/2, \\ \tanh(\kappa(3/4 - y)), & y > 1/2, \end{cases} \qquad (99)$$
$$u_y = \delta \sin(2\pi(x + 1/4)),$$

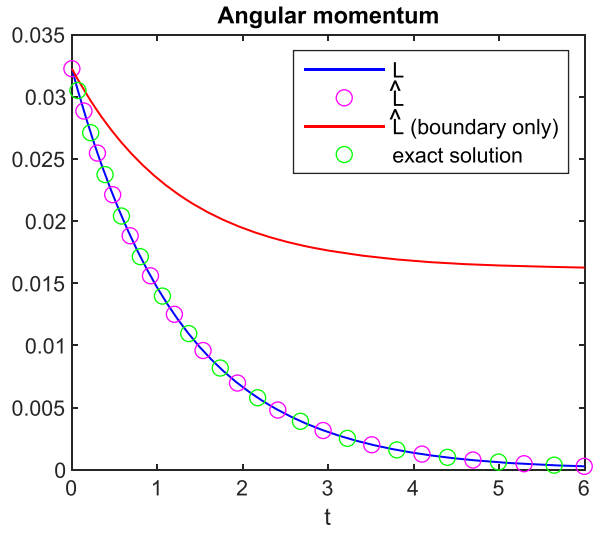


**FIG. 3.** Angular momentum decays at a rate given by the sum of the boundary and interior torques, not by the boundary torque alone.

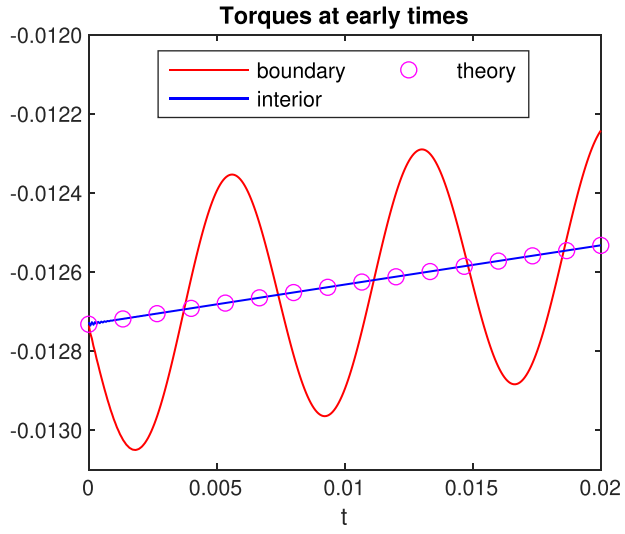


**FIG. 4.** Two discrete torques at early times. The boundary torque shows resolved acoustic oscillations, but the interior torque from $\boldsymbol{\epsilon} : \boldsymbol{\Pi}$ does not.

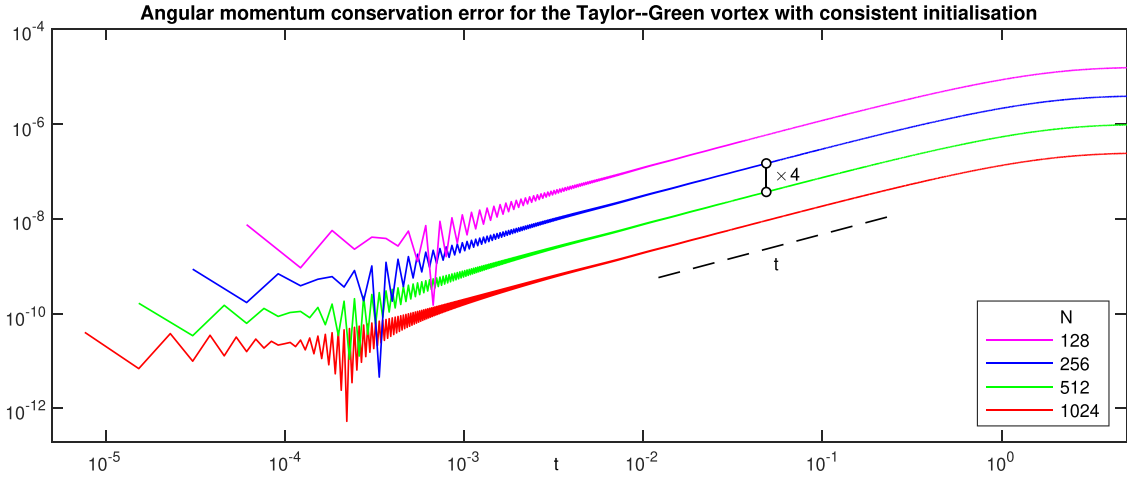


**FIG. 5.** Difference between $L(t)$ and $\hat{L}(t)$ for the symmetrized formulation with the boundary torque alone grows linearly with time, but decreases like $1/N^2$ with increasing resolution at fixed Mach number.

with parameters $\kappa = 80$ and $\delta = 0.05$ in the domain $(x, y) \in [0, 1]^2$ with periodic boundary conditions. The initial density field was again chosen to satisfy

$$c_s^2 \nabla^2 \rho + \rho_0 \nabla\nabla : (\boldsymbol{uu}) = 0, \tag{100}$$

with $\rho$ computed using discrete Fourier transforms.

The sinusoidal perturbation $u_y$ triggers a Kelvin–Helmholtz instability in the two anti-parallel shear layers, which subsequently roll up into two spiral vortices as shown in Fig. 8 for a simulation with $\nu = 10^{-3}$ and Ma $= 1/128$. The vorticity fields in Fig. 8 were computed from the $\mathbf{g}_i$ in the symmetrized formulation using (70). Figure 9 shows that the vorticity fields computed using (70) converge toward the vorticity fields computed by spectrally differentiating the velocity field. The errors on an $N \times N$ lattice are $O(1/N^2)$ in the diffusive scaling that lowers the Mach number as $N$ increases, here taking Ma $= 1/N$. This scaling balances the spatial truncation error with the compressibility error and also with the error due to neglecting higher-order terms in the Chapman–Enskog expansion of the momentum flux in Sec. IV B.

The vortex roll-up leads to an accumulation of (negative) angular momentum in the bottom-left quadrant of the simulation domain, as shown in Fig. 10. The evolving angular momentum $L(t)$ is in excellent visual agreement with the integrated boundary torque $\hat{L}(t)$ for the symmetrized scheme. The integrated boundary torque for the unsymmetrised scheme initially has quite good agreement but later deviates significantly. This is because the initial behavior is dominated by the



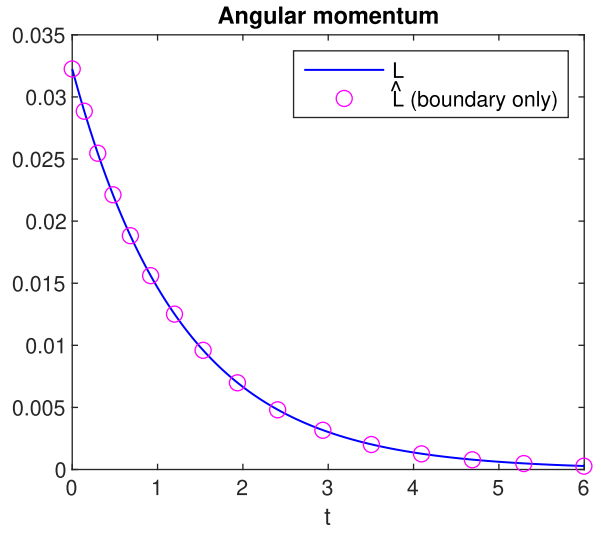


**FIG. 6.** Angular momentum decays as expected in the symmetrized formulation, at a rate given by the boundary torque alone.

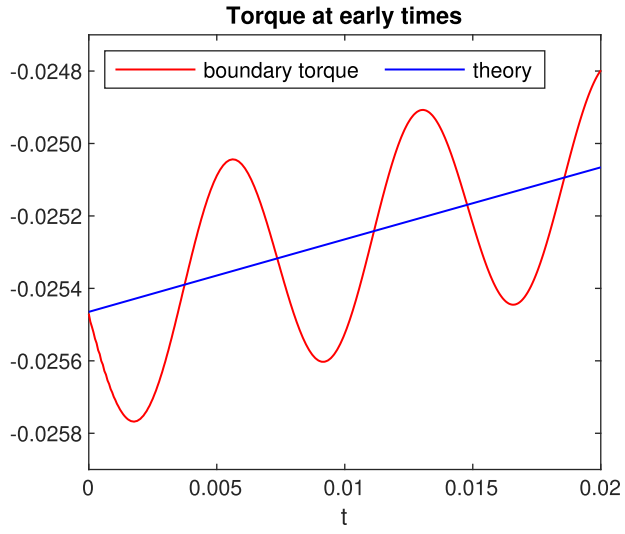


**FIG. 7.** Numerical boundary torque in the symmetrized formulation at early times showing resolved acoustic oscillations.

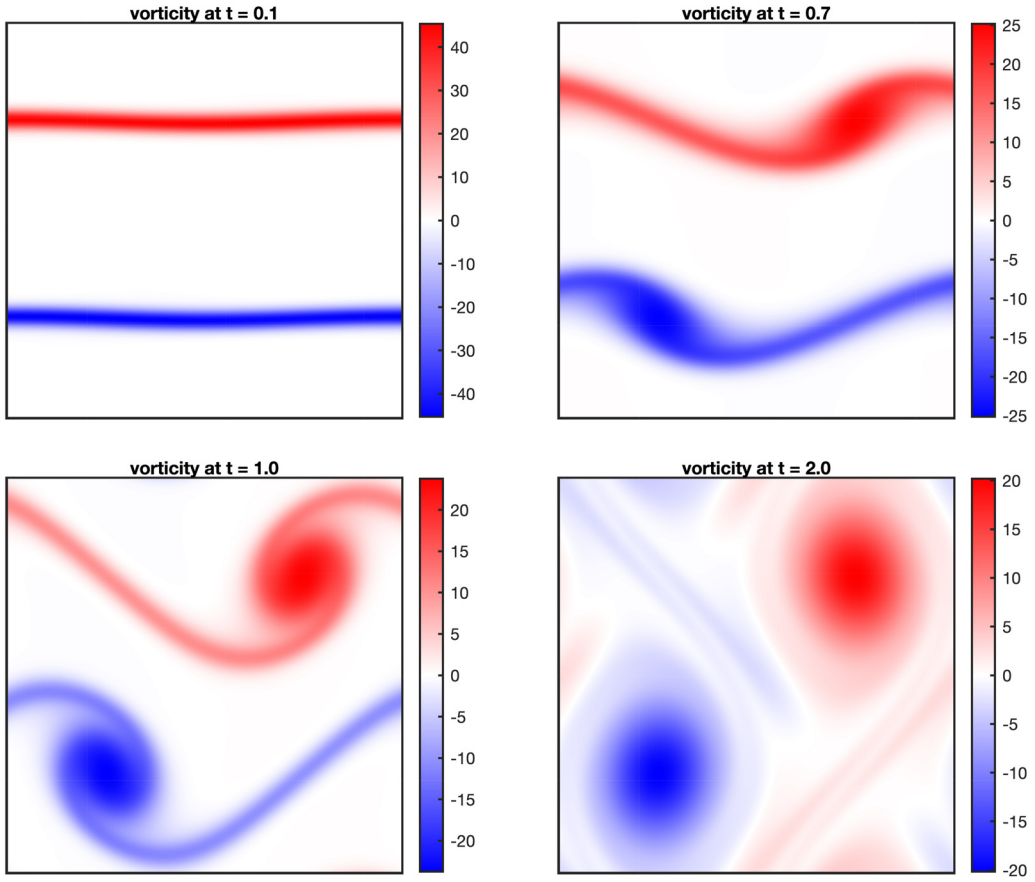


**FIG. 8.** Vorticity fields computed from the $\mathbf{g}_i$ using (70) at times 0.1, 0.7, 1.0, and 2.0 for a simulation with $\nu = 0.001$ and $Ma = 1/128$ on a $512 \times 512$ lattice.

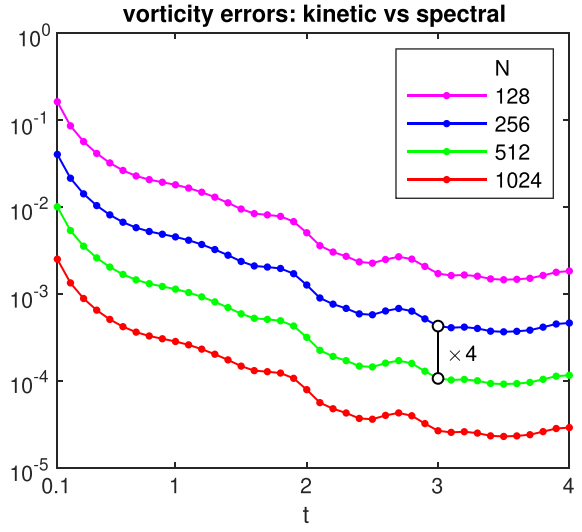


**FIG. 9.** Differences between the vorticity fields calculated from the $\mathbf{g}_i$ using (70) and from spectrally differentiating the velocity field. The differences at $t = 0$, not shown, are much smaller because $\mathbf{\Pi}$ is initialized from $\nabla \mathbf{u}$.

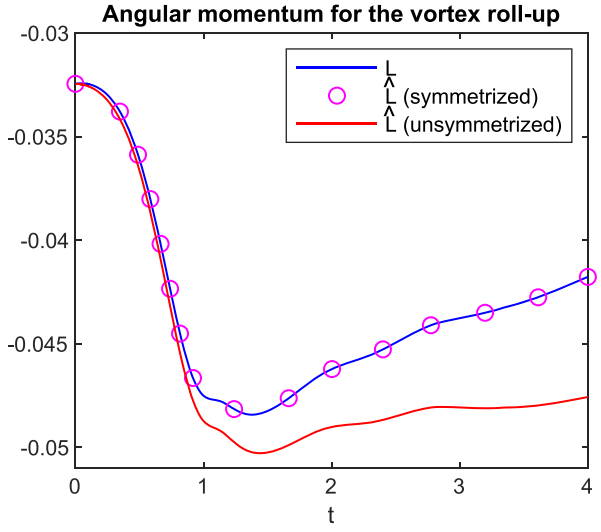


**FIG. 10.** Angular momentum $L$ compared with the integrated boundary torque $\hat{L}$ for the symmetrized and unsymmetrised schemes. The former matches, but the latter does not.

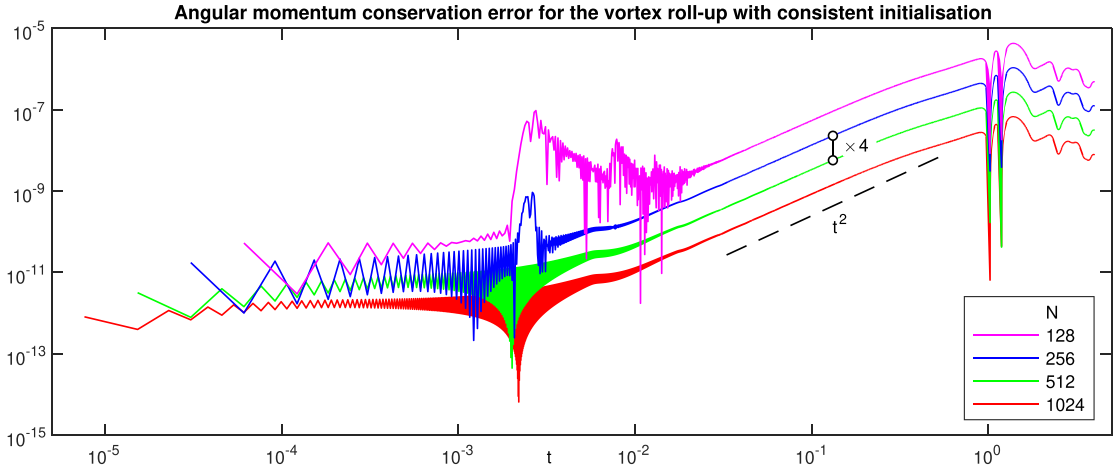


**FIG. 11.** Difference between $L(t)$ and $\hat{L}(t)$ with consistent initialization. The difference decreases as $O(1/N^2)$ with increasing resolution but grows like $t^2$ during the linear phase of the instability. The consistent initialization greatly reduces the amplitude of the initial oscillations.

torque due to the advective part of the momentum flux, which is always symmetric. The contribution from the asymmetric viscous momentum flux only appears at later times.

Figure 11 shows the evolution in time of the difference between the instantaneous discrete angular momentum $L(t)$ in the quadrant $[0, 1/2]^2$ and the integrated boundary torque $\hat{L}(t)$ for simulations using the symmetrized scheme with a consistent initialization using the analytical expression for $\nabla\mathbf{u}$ at $t = 0$. The difference decreases as $O(1/N^2)$ with increasing spatial resolution $N$ at fixed Mach number $\mathrm{Ma} = 1/128$. The difference also grows like $t^2$ during the linear phase of the Kelvin–Helmholtz instability. The irregular oscillations roughly between $t = 10^{-3}$ and $t = 10^{-2}$ for the two coarsest lattices ($N = 128$ and $N = 256$) appear to be due to the shear layers not being properly resolved at these coarse resolutions. They are completely absent for $N \geq 512$.

Figure 12 shows the equivalent evolution for the symmetrized scheme with the distribution functions initialized to the equilibrium distributions, without the $\nabla\mathbf{u}$ correction. The difference again decreases as $O(1/N^2)$ with increasing spatial resolution $N$ at fixed Mach number $\mathrm{Ma} = 1/128$, but there are much larger zig–zag oscillations from time step to time step. These are suppressed by about a factor of $10^4$ by the consistent initialization, although the suppression is not perfect because the analytical expression for $\nabla\mathbf{u}$ does not exactly match the discrete approximation to $\nabla\mathbf{u}$ that emerges from the numerical scheme.

## IX. CONCLUSIONS

Lattice Boltzmann formulations of hydrodynamics represent the fluid using distributions of particles, each moving with one of a small set of constant velocities. The standard formulations treat the particles

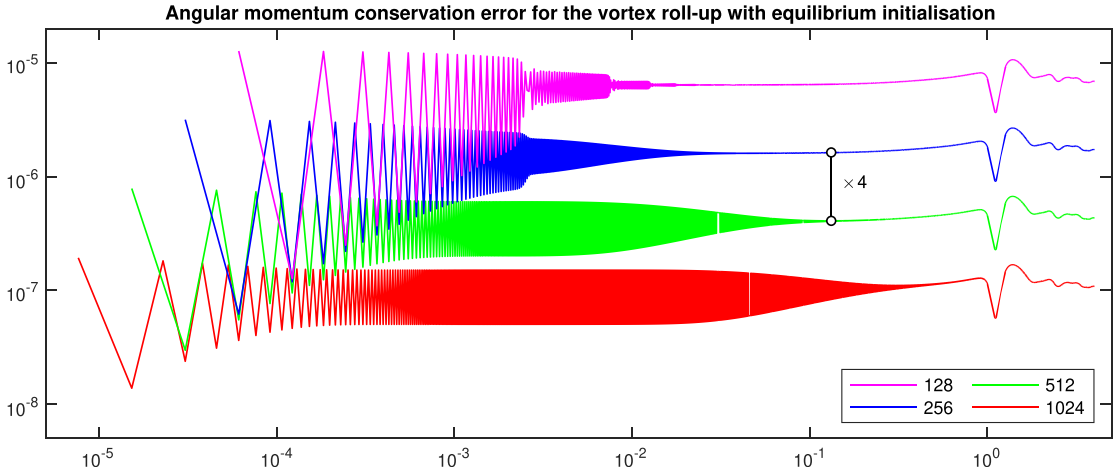


**FIG. 12.** Difference between $L(t)$ and $\hat{L}(t)$ with equilibrium initialization. The difference decreases as $O(1/N^2)$ with increasing resolution but has large amplitude zig–zag oscillations due to the inconsistent initialization.

as points carrying momentum in their direction of motion. The distribution functions are then scalar fields, the momentum density is a vector field, and the momentum flux is a symmetric tensor field. Conservation of linear momentum thus implies conservation of angular momentum.

The vector lattice Boltzmann formulation treats each particle as carrying a momentum vector that may not be aligned with its direction of motion. The momentum flux tensor $\mathbf{\Pi}$ is then in general not symmetric. There is an additional volume torque proportional to the antisymmetric part of $\mathbf{\Pi}$ in the evolution equation for angular momentum. This can be removed using a collision operator that applies separate relaxation times to the symmetric and antisymmetric parts of the momentum flux tensor and then sets the relaxation time for the antisymmetric part to zero. When discretized, this implies a marginally stable over-relaxation that reverses the sign of the antisymmetric part of the momentum flux at every collision. The average of the pre-collision and post-collision momentum fluxes is symmetric. This scheme can be interpreted as an analog of the Chorin–Temam projection scheme, one that projects the momentum flux onto the space of symmetric tensors. The construction of initial conditions that are consistent with the gradient of the initial velocity field, and the local computation of the vorticity field from the non-equilibrium distribution functions, have been formulated using the discrete collision operator and the discrete momentum flux. These objects remain well behaved when the antisymmetric relaxation time is set to zero, even though the underlying continuous collision operator does not.

The vector lattice Boltzmann formulation with this symmetrizing collision operator satisfies the usual angular momentum conservation law to second-order accuracy under spatial refinement at fixed Mach number. The vorticity field computed from the non-equilibrium distribution functions converges with second-order accuracy to the vorticity field computed by spectrally differentiating the velocity field provided we use a diffusive scaling that lowers the Mach number as we refine the spatial lattice. This represents a significant advantage of the vector formulation, as only the symmetric strain rate can be computed locally at lattice points in scalar lattice Boltzmann formulations of hydrodynamics.

## ACKNOWLEDGMENTS

The computations employed the Advanced Research Computing facilities at the University of Oxford.[77]

## AUTHOR DECLARATIONS

### Conflict of Interest

The authors have no conflicts to disclose.

### Author Contributions

**Paul J. Dellar:** Conceptualization (equal); Formal analysis (equal); Investigation (equal); Methodology (equal); Software (equal); Visualization (equal); Writing – original draft (equal); Writing – review & editing (equal).

## DATA AVAILABILITY

The data used to create the figures are available from the University of Oxford Research Archive.

## APPENDIX: PARAMETER CONSTRAINTS FROM A STABILITY STRUCTURE

Most scalar lattice Boltzmann schemes satisfy a "stability structure" that establishes the linear stability of perturbations around the global equilibria $f_i^{(0)}$ for a uniform rest state with $\rho = \rho_0$ and $\mathbf{u} = 0$. The Jacobian matrix of the linearized scalar lattice Boltzmann scheme is used to construct a weighted $\ell^2$ norm of $f_i - f_i^{(0)}$ that serves as a Lyapunov function for the discrete system.[14,78,79]

Carfora and Natalini[23] showed, using results from Bouchut,[21] that the vector discrete kinetic system in Sec. IV satisfies a more general stability result. The Jacobian matrices of the equilibrium distribution functions with respect to the conserved moments have non-negative real eigenvalues when

$$1/\lambda < 2a < 1/2. \tag{A1}$$

These conditions imply $\lambda^2 > \lambda > 2$ so the diffusivity $\tau(2a\lambda^2 - 1)$ is positive in the Chapman–Enskog expansion of the density equation in Sec. IV A.

Zhao[24] combined these approaches to form a stability structure for the vector case. This relies on the Jacobian matrices of the individual vector equilibrium distributions $\mathbf{F}_i^{(0)} = (f_i^{(0)}, \mathbf{g}_i^{(0)})$ with respect to the conserved moments $\mathbf{w} = (\rho, m_x, m_y)$ evaluated at the rest state $\rho = \rho_0$, $\mathbf{m} = 0$ being symmetric and positive definite. The five Jacobian matrices are all symmetric and independent of the value of $\rho_0$

$$\frac{\partial \mathbf{F}_0^{(0)}}{\partial \mathbf{w}} = \begin{pmatrix} 1-4a & 0 & 0 \\ 0 & 1-4a & 0 \\ 0 & 0 & 1-4a \end{pmatrix}, \tag{A2a}$$

$$\frac{\partial \mathbf{F}_1^{(0)}}{\partial \mathbf{w}} = \begin{pmatrix} a & 1/(2\lambda) & 0 \\ 1/(2\lambda) & a & 0 \\ 0 & 0 & a \end{pmatrix}, \tag{A2b}$$

$$\frac{\partial \mathbf{F}_3^{(0)}}{\partial \mathbf{w}} = \begin{pmatrix} a & -1/(2\lambda) & 0 \\ -1/(2\lambda) & a & 0 \\ 0 & 0 & a \end{pmatrix}, \tag{A2c}$$

$$\frac{\partial \mathbf{F}_2^{(0)}}{\partial \mathbf{w}} = \begin{pmatrix} a & 0 & 1/(2\lambda) \\ 0 & a & 0 \\ 1/(2\lambda) & 0 & a \end{pmatrix}, \tag{A2d}$$

$$\frac{\partial \mathbf{F}_4^{(0)}}{\partial \mathbf{w}} = \begin{pmatrix} a & 0 & -1/(2\lambda) \\ 0 & a & 0 \\ -1/(2\lambda) & 0 & a \end{pmatrix}. \tag{A2e}$$

The first matrix $\partial \mathbf{F}_0^{(0)}/\partial \mathbf{w}$ is positive definite when $a < 1/4$. The remaining four matrices have the eigenvalues $a$ and $a \pm 1/(2\lambda)$, so they are all positive definite when $a > 1/(2\lambda)$.

Baty *et al.*[25] used a vector lattice Boltzmann scheme on the D2Q4 lattice that omits the rest particles with $i = 0$. This is equivalent to choosing $a = 1/4$. The stability result then holds for the remaining matrices $\partial \mathbf{F}_i^{(0)}/\partial \mathbf{w}$ with $i = 1, 2, 3, 4$.

## REFERENCES

[1]L. Euler, "Nova methodus motum corporum rigidorum determinandi," Novi Comm. Acad. Sci. Petrop. **20**, 208 (1775).
[2]C. Truesdell, "Zusammenfassender Bericht Die Entwicklung des Drallsatzes," Z. Angew. Math. Mech. **44**, 149 (1964).

[3]C. Truesdell, *Essays in the History of Mechanics* (Springer, Berlin, Heidelberg, 1968).
[4]W. H. Müller, W. Rickert, and E. N. Vilchevskaya, "Thence the moment of momentum," Z. Angew. Math. Mech. **100**, e202000117 (2020).
[5]G. Hamel, "Über die Grundlagen der Mechanik," Math. Ann. **66**, 350 (1908).
[6]L. Boltzmann, *Populäre Schriften*, edited by J. A. Barth (Leipzig, 1905), pp. 253–307.
[7]C. Truesdell and R. Toupin, "The classical field theories," in *Principles of Classical Mechanics and Field Theory*, edited by S. Flügge (Springer, Berlin, Heidelberg, 1960), pp. 226–858.
[8]G. G. Stokes, "Report on double refraction," in *Report of the British Association for the Advancement of Science* (John Murray, London, 1863), pp. 253–282.
[9]G. K. Batchelor, *An Introduction to Fluid Dynamics* (Cambridge University Press, Cambridge, 1967).
[10]W. Thomson, "On a gyrostatic a dynamic constitution for 'ether'," P. R. Soc. Edinb. **17**, 127 (1890).
[11]R. Benzi, S. Succi, and M. Vergassola, "The lattice Boltzmann equation: Theory and applications," Phys. Rep. **222**, 145 (1992).
[12]T. Krüger, H. Kusumaatmaja, A. Kuzmin, O. Shardt, G. Silva, and E. M. Viggen, *The Lattice Boltzmann Method* (Springer, 2017).
[13]S. Succi, *The Lattice Boltzmann Equation: For Complex States of Flowing Matter* (Oxford University Press, Oxford, 2018).
[14]P. Lallemand, L.-S. Luo, M. Krafczyk, and W.-A. Yong, "The lattice Boltzmann method for nearly incompressible flows," J. Comput. Phys. **431**, 109713 (2021).
[15]D. O. Martínez, S. Chen, and W. H. Matthaeus, "Lattice Boltzmann magnetohydrodynamics," Phys. Plasmas **1**, 1850 (1994).
[16]M. Mendoza and J. D. Muñoz, "Three-dimensional lattice Boltzmann model for magnetic reconnection," Phys. Rev. E **77**, 026713 (2008).
[17]P. J. Dellar, "Lattice kinetic schemes for magnetohydrodynamics," J. Comput. Phys. **179**, 95 (2002).
[18]P. J. Dellar, "Electromagnetic waves in lattice Boltzmann magnetohydrodynamics," Europhys. Lett. **90**, 50002 (2010).
[19]P. J. Dellar, "Lattice Boltzmann magnetohydrodynamics with current-dependent resistivity," J. Comput. Phys. **237**, 115 (2013).
[20]P. J. Dellar, "Hyperbolic divergence cleaning in lattice Boltzmann magnetohydrodynamics," Commun. Comput. Phys. **33**, 245 (2023).
[21]F. Bouchut, "Construction of BGK models with a family of kinetic entropies for a given system of conservation laws," J. Stat. Phys. **95**, 113 (1999).
[22]P. J. Dellar, "Vector lattice Boltzmann equations: From magnetohydrodynamics to active matter," in *Progress in Industrial Mathematics at ECMI 2021*, edited by M. Ehrhardt and M. Günther (Springer, Cham, 2022), pp. 407–416.
[23]M. F. Carfora and R. Natalini, "A discrete kinetic approximation for the incompressible Navier-Stokes equations," ESAIM: M2AN. **42**, 93 (2008).
[24]J. Zhao, "Discrete-velocity vector-BGK models based numerical methods for the incompressible Navier–Stokes equations," Commun. Comput. Phys. **29**, 420 (2021).
[25]H. Baty, F. Drui, P. Helluy, E. Franck, C. Klingenberg, and L. Thanhäuser, "A robust and efficient solver based on kinetic schemes for magnetohydrodynamics (MHD) equations," Appl. Math. Comput. **440**, 127667 (2023).
[26]G. Wissocq, Y. Liu, and R. Abgrall, "A positive- and bound-preserving vectorial lattice Boltzmann method in two dimensions," arXiv:2411.15001 (2024).
[27]F. Dubois, "Simulation of strong nonlinear waves with vectorial lattice Boltzmann schemes," Int. J. Mod. Phys. C **25**, 1441014 (2014).
[28]B. Graille, "Approximation of mono-dimensional hyperbolic systems: A lattice Boltzmann scheme as a relaxation method," J. Comput. Phys. **266**, 74 (2014).
[29]A. Malevanets and R. Kapral, "Mesoscopic model for solvent dynamics," J. Chem. Phys. **110**, 8605 (1999).
[30]A. Malevanets and R. Kapral, "Solute molecular dynamics in a mesoscale solvent," J. Chem. Phys. **112**, 7260 (2000).
[31]G. Gompper, T. Ihle, D. M. Kroll, and R. G. Winkler, "Multi-particle collision dynamics: A particle-based mesoscale simulation approach to the hydrodynamics of complex fluids," Adv. Polym. Sci. **221**, 1 (2008).
[32]T. Ihle and D. M. Kroll, "Stochastic rotation dynamics. I. Formalism, Galilean invariance, and Green-Kubo relations," Phys. Rev. E **67**, 066705 (2003).
[33]T. Ihle and D. M. Kroll, "Stochastic rotation dynamics. II. Transport coefficients, numerics, and long-time tails," Phys. Rev. E **67**, 066706 (2003).
[34]C. M. Pooley and J. M. Yeomans, "Kinetic theory derivation of the transport coefficients of stochastic rotation dynamics," J. Phys. Chem. B **109**, 6505 (2005).
[35]T. Ihle, E. Tüzel, and D. M. Kroll, "Equilibrium calculation of transport coefficients for a fluid-particle model," Phys. Rev. E **72**, 046707 (2005).
[36]I. O. Götze, H. Noguchi, and G. Gompper, "Relevance of angular momentum conservation in mesoscale hydrodynamics simulations," Phys. Rev. E **76**, 046705 (2007).
[37]D. Coulette, E. Franck, P. Helluy, M. Mehrenberger, and L. Navoret, "High-order implicit palindromic discontinuous Galerkin method for kinetic-relaxation approximation," Comput. Fluids **190**, 485 (2019).
[38]A. J. Chorin, "Numerical solution of the Navier–Stokes equations," Math. Comp. **22**, 745 (1968).
[39]R. Témam, "Sur l'approximation de la solution des équations de Navier-Stokes par la méthode des pas fractionnaires (II)," Arch. Ration. Mech. Anal. **33**, 377 (1969).
[40]J. S. Dahler and L. E. Scriven, "Theory of structured continua. I. General consideration of angular momentum and polarization," Proc. R. Soc. London A **275**, 504 (1963).
[41]R. E. Rosensweig, *Ferrohydrodynamics* (Cambridge University Press, Cambridge, 1985).
[42]H. Grad, "Statistical mechanics, thermodynamics, and fluid dynamics of systems with an arbitrary number of integrals," Comm. Pure Appl. Math. **5**, 455 (1952).
[43]J. L. Ericksen, "Anisotropic fluids," Arch. Ratl. Mech. Anal. **4**, 231 (1959).
[44]J. S. Dahler and L. E. Scriven, "Angular momentum of continua," Nature **192**, 36 (1961).
[45]S. Feng, A. L. Graham, J. R. Abbott, and H. Brenner, "Antisymmetric stresses in suspensions: Vortex viscosity and energy dissipation," J. Fluid Mech. **563**, 97 (2006).
[46]C. F. Curtiss, "Kinetic theory of nonspherical molecules," J. Chem. Phys. **24**, 225 (1956).
[47]J. S. Dahler, "Transport phenomena in a fluid composed of diatomic molecules," J. Chem. Phys. **30**, 1447 (1959).
[48]S. R. de Groot and P. Mazur, *Non-Equilibrium Thermodynamics* (North-Holland, Amsterdam, 1962).
[49]D. W. Condiff and J. S. Dahler, "Fluid mechanical aspects of antisymmetric stress," Phys. Fluids **7**, 842 (1964).
[50]M. I. Shliomis, "Hydrodynamics of a liquid with intrinsic rotation," Sov. Phys. JETP **24**, 173 (1967).
[51]Y. Wu, H. L. Tepper, and G. A. Voth, "Flexible simple point-charge water model with improved liquid-state properties," J. Chem. Phys. **124**, 024503 (2006).
[52]J. S. Hansen, H. Bruus, B. D. Todd, and P. J. Daivis, "Rotational and spin viscosities of water: Application to nanofluidics," J. Chem. Phys. **133**, 144906 (2010).
[53]L. D. Landau and E. M. Lifshitz, *Fluid Mechanics*, 2nd ed. (Pergamon, Oxford, 1987).
[54]P. L. Bhatnagar, E. P. Gross, and M. Krook, "A model for collision processes in gases. I. Small amplitude processes in charged and neutral one-component system," Phys. Rev. **94**, 511 (1954).
[55]N. G. van Kampen, "Elimination of fast variables," Phys. Rept. **124**, 69 (1985).
[56]N. G. van Kampen, "Chapman–Enskog as an application of the method for eliminating fast variables," J. Stat. Phys. **46**, 709 (1987).
[57]P. J. Dellar, "Macroscopic descriptions of rarefied gases from the elimination of fast variables," Phys. Fluids **19**, 107101 (2007).
[58]S. Hou, Q. Zou, S. Chen, G. D. Doolen, and A. C. Cogley, "Simulation of cavity flow by the lattice Boltzmann method," J. Comput. Phys. **118**, 329 (1995).
[59]M. Hénon, "Viscosity of a lattice gas," Complex Syst. **1**, 763 (1987).
[60]G. Strang, "On the construction and comparison of difference schemes," SIAM J. Numer. Anal. **5**, 506 (1968).
[61]P. J. Dellar, "An interpretation and derivation of the lattice Boltzmann method using Strang splitting," Comput. Math. Appl. **65**, 129 (2013).
[62]X. He, S. Chen, and G. D. Doolen, "A novel thermal model of the lattice Boltzmann method in incompressible limit," J. Comput. Phys. **146**, 282 (1998).
[63]R. A. Brownlee, A. N. Gorban, and J. Levesley, "Stability and stabilization of the lattice Boltzmann method," Phys. Rev. E **75**, 036711 (2007).

[64]E. Aharonov and D. H. Rothman, "Non-Newtonian flow through porous media—A lattice Boltzmann method," Geophys. Res. Lett. **20**, 679–682, https://doi.org/10.1029/93GL00473 (1993).
[65]N. Rakotomalala, D. Salin, and P. Watzky, "Simulations of viscous flows of complex fluids with a Bhatnagar, Gross, and Krook lattice gas," Phys. Fluids **8**, 3200 (1996).
[66]T. N. Phillips and G. W. Roberts, "Lattice Boltzmann models for non-Newtonian flows," IMA J. Appl. Math. **76**, 790 (2011).
[67]J. Smagorinsky, "General circulation experiments with the primitive equations," Mon. Wea. Rev. **91**, 99 (1963).
[68]J. A. Somers, "Direct simulation of fluid flow with cellular automata and the lattice-Boltzmann equation," Appl. Sci. Res. **51**, 127 (1993).
[69]S. Hou, J. D. Sterling, C. Chen, and G. D. Doolen, "A lattice Boltzmann subgrid model for high Reynolds number flows," in *Pattern Formation and Lattice Gas Automata*, Fields Institute Proceedings Vol. 6, edited by A. T. Lawniczak and R. Kapral (AMS, 1996), pp. 151–166.
[70]P. A. Skordos, "Initial and boundary conditions for the lattice Boltzmann method," Phys. Rev. E **48**, 4823 (1993).
[71]P. M. Gresho, "Incompressible fluid dynamics: Some fundamental formulation issues," Annu. Rev. Fluid Mech. **23**, 413 (1991).
[72]F. Aurenhammer, "Voronoi diagrams—A survey of a fundamental geometric data structure," ACM Comput. Surv. **23**, 345 (1991).
[73]G. I. Taylor and A. E. Green, "Mechanism of the production of small eddies from large ones," Proc. R. Soc. London, Ser. A **158**, 499 (1937).
[74]C. E. Pearson, "A computational method for viscous flow problems," J. Fluid Mech. **21**, 611 (1965).
[75]J. B. Bell, P. Colella, and H. M. Glaz, "A second-order projection method for the incompressible Navier–Stokes equations," J. Comput. Phys. **85**, 257 (1989).
[76]M. L. Minion and D. L. Brown, "Performance of under-resolved two-dimensional incompressible flow simulations, II," J. Comput. Phys. **138**, 734 (1997).
[77]A. Richards (2015). "University of Oxford Advanced Research Computing," Zenodo. https://doi.org/10.5281/zenodo.22558
[78]M. K. Banda, W.-A. Yong, and A. Klar, "A stability notion for lattice Boltzmann equations," SIAM J. Sci. Comput. **27**, 2098 (2006).
[79]M. Junk and W.-A. Yong, "Weighted $\mathbb{L}^2$-stability of the lattice Boltzmann method," SIAM J. Numer. Anal. **47**, 1651 (2009).